



Decoding primary forest changes in Haiti and the Dominican Republic using Landsat time series

Falu Hong^{a,*}, S. Blair Hedges^b, Zhiqiang Yang^c, Ji Won Suh^a, Shi Qiu^a, Joel Timyan^d, Zhe Zhu^a

^a Department of Natural Resources and the Environment, University of Connecticut, Storrs, CT 06269, USA

^b Center for Biodiversity, Temple University, 1925 N 12th Street, Suite 502, Philadelphia, PA 19122, USA

^c US Forest Service, Rocky Mountain Research Station, Riverdale, UT, USA

^d Haiti National Trust, #20, rue Faubert, Suite 3, Pétionville, Haiti

ARTICLE INFO

Edited by Marie Weiss

Keywords:

Primary forest
Land cover
Landsat
Disturbance
Resilience
Haiti
The Dominican Republic

ABSTRACT

Forest loss has greatly reduced habitats and threatened Earth's biodiversity. Primary forest (PF) has an irreplaceable role in supporting biodiversity compared with secondary forest (SF). Therefore, distinguishing PF and SF using remote sensing observations is critical for evaluating the impact of forest loss on biodiversity. However, continuous monitoring of PF loss through remote sensing time series observations remains largely unexplored, particularly in developing tropical regions. In this study, we used the COLD algorithm (Continuous monitoring of Land Disturbance) and Landsat time series data to quantify PF loss on the island of Hispaniola, comprising Haiti and the Dominican Republic, from 1996 to 2022. We considered the resilience of PF to different disturbance agents and identified the primary drivers of PF loss in Hispaniola through a sample-based approach. Accuracy assessment based on the stratified random sample shows that the overall accuracy of land cover classification is 80.5% ($\pm 5.2\%$) [95% confidence interval]. The user's, producer's, and overall accuracies of PF loss detection are 68.8% ($\pm 9.3\%$), 73.6% ($\pm 38\%$), and 99.4% ($\pm 0.5\%$), respectively. Map-based analysis reveals a more pronounced decline in PF coverage in Haiti (0.75% to 0.44% at 324 ha/year) compared to the Dominican Republic (7.14% to 5.67% at 2,704 ha/year), with substantial PF loss occurring both inside and outside protected areas. Furthermore, Haiti exhibits a higher degree of PF fragmentation, characterized by smaller and fewer PF patches, than the Dominican Republic, posing significant challenges for biodiversity conservation. The remaining PFs are found on steeper slopes in both Haiti and the Dominican Republic, suggesting that flatter, more accessible areas are more vulnerable to PF loss. Fire, tree-cutting, and hurricanes were identified as the primary drivers of PF loss, accounting for 65.7%, 20.9%, and 9.0% of the PF loss area in Hispaniola, respectively. These findings underscore the urgent need for conservation policies to protect remaining PF in Hispaniola, particularly in Haiti.

1. Introduction

Habitat loss, driven by human activities and climate change, poses a major threat to global biodiversity (Alroy, 2017; Brooks et al., 2002). Among forest ecosystems, primary forest (PF), also often referred to as old-growth forest, stands out for its irreplaceable role in supporting biodiversity, offering unique ecological niches and harboring a disproportionately high number of endemic species compared to secondary forest (SF) (Barlow et al., 2007; Gibson et al., 2011; Hedges et al., 2018; Martin et al., 2004). While remote sensing observations have called attention to the widespread forest degradation and deforestation

(Hansen et al., 2013), accurately assessing the impact of forest loss on biodiversity necessitates differentiating between PF and SF. This distinction, however, remains a persistent challenge, especially in the highly biodiverse yet data-scarce tropical regions. Existing PF maps often suffer from inconsistencies due to varying definitions and methodologies. Some studies rely on strict spatial criteria (size and length), rendering PF virtually absent on small islands, while others define PF as undisturbed forest within a Landsat time series, potentially including old secondary forest (Turubanova et al., 2018; Vancutsem et al., 2021). Localized mapping efforts frequently employ their own definitions based on local expert knowledge, sometimes using terms like intact forest or

* Corresponding author.

E-mail address: faluhong@uconn.edu (F. Hong).

<https://doi.org/10.1016/j.rse.2024.114590>

Received 26 June 2024; Received in revised form 21 December 2024; Accepted 23 December 2024

Available online 8 January 2025

0034-4257/© 2025 The Authors. Published by Elsevier Inc. This is an open access article under the CC BY license (<http://creativecommons.org/licenses/by/4.0/>).

old-growth forest interchangeably (Arévalo et al., 2020; Decuyper et al., 2022; Kormos et al., 2018; Mikoláš et al., 2023; Turubanova et al., 2018; Wang et al., 2019). These discrepancies hinder intercomparison and create challenges for large-scale, standardized mapping.

The widely used qualitative definition of PF, provided by the Food and Agriculture Organization (FAO), describes it as “naturally regenerated forest of native species where there are no clearly visible indications of human activities and the ecological processes are not significantly disturbed” (FAO, 2015). Previous studies have used similar PF definitions based on the FAO (Food and Agriculture Organization) definition (Bernier et al., 2017; Kormos et al., 2018; Mikoláš et al., 2019; Sabatini et al., 2021), including two key criteria. First, tree canopy cover should be dense enough to support biodiversity. For example, recent studies have used relatively high tree canopy thresholds for PF, with thresholds ranging from 60% to 100% (Hedges et al., 2018; Rodrigues-Eklund et al., 2021; Turubanova et al., 2018). Second, PF should exhibit an ecosystem structure and function that remains minimally disturbed.

PFs include pristine PFs, which are free of disturbance, and recovered PFs, which have experienced disturbances but the original ecosystem structure and functions remain intact or quickly recover after disturbances (FAO, 2015). Pristine PFs are often in remote regions that are inaccessible to human activities or well protected. Recovered PFs demonstrate their ability to maintain their pre-disturbance forest structure and ecosystem functions after a disturbance, provided it does not exceed the PF's short-term resilience capacity (ITTO, 2002). For instance, PFs may recover from minor and short events (Knorn et al., 2013), such as flash droughts or weak hurricanes, within a few years. However, recovery from human-induced or severe disturbances such as low-intensity tree-cutting or severe wildfires, landslides, and hurricanes can take much longer, often over fifty years, and may result in irreversible damage, transforming PFs into degraded PFs or other land cover types, such as SFs (Heinrich et al., 2023; Poorter et al., 2016). Degraded PFs denote that PFs have been severely impacted and cannot maintain their original ecosystem structure and functions after disturbances. They represent a transition stage and usually lead to replacement with SFs. Consequently, degraded PFs are typically considered a subset of SFs. In this study, we will refer to both degraded PFs and SFs collectively as SFs hereafter.

While previous studies have identified key features of PFs, the current qualitative definition by the FAO poses practical challenges in identifying PFs (Bernier et al., 2017). Remote sensing provides a quantitative approach to determining tree canopy cover, and long-term time series observations can be used to quantify disturbance agents and their intensity, as well as to measure forest recovery through spectral signatures (Hansen et al., 2013; Vancutsem et al., 2021; Wang et al., 2019; White et al., 2017; Zhu et al., 2022). These insights are valuable for distinguishing different forest conditions, including pristine PF, recovered PF, and SF. Therefore, a workflow based on remote sensing time series has the potential to establish a standardized method for identifying PF at large scales (Vancutsem et al., 2021; Wang et al., 2020).

The island of Hispaniola, comprising Haiti and the Dominican Republic, was once predominantly covered by PFs, but now faces significant pressure of biodiversity loss due to deforestation (Álvarez-Berríos et al., 2013; Myers et al., 2000). Deforestation can cause forest fragmentation, which then facilitates additional deforestation through edge effects and greater exposure to wind (Laurance et al., 1997). Haiti has experienced a dramatic loss of its PFs, as detailed by Hedges et al. (2018). The tree-cutting of forests during colonial times, shifting cultivation, poor conservation policy, frequent natural disasters, such as earthquakes and hurricanes, and climate change have caused the decline of PF (Cohen, 1984; Hedges et al., 2018). Although Haiti and the Dominican Republic share similar natural environment backgrounds, there is a substantial disparity in the PF distribution and change pattern between Haiti and the Dominican Republic due to differences in the present economic status, historical population structure, and land management policy (Wilson et al., 2001). This PF disparity is also

manifested in the differences of PF fragmentation level, the effectiveness of PF-protected areas, and the major drivers of PF loss. Continuous mapping of Hispaniola's PFs using a time series from remote sensing can reveal PF disparities between Haiti and the Dominican Republic and concurrently monitor their distinct trends of PF loss.

However, most previous studies on Hispaniola have largely focused on overall forest cover change, often failing to distinguish between PF and SF. This lack of discrimination has led to various, sometimes contradictory findings on whether the forest cover is increasing or decreasing in Haiti (Churches et al., 2014; Pauleus and Aide, 2020; Rodrigues-Eklund et al., 2021) and the Dominican Republic (John and Yolanda, 2019; Sangermano et al., 2015a). Such discrepancies arise from varying definitions of land cover categories and the mixing of PF and SF (Aide et al., 2013; Álvarez-Berríos et al., 2013). Only two previous published studies have analyzed PF change in Haiti and one study reported PF change in the Dominican Republic. Both of them reported PF loss in the two countries. Cohen (1984) reported extensive PF loss in Haiti and projected the complete loss of PF before 2000 using aerial photogrammetry between 1956 and 1976. Hedges et al. (2018) used Landsat imagery and time-series analysis to study the loss of PF, finding less than 1% of PF in Haiti since 2000. The Global Forest Watch project mapped the pan-tropical PF in 2001 based on the training knowledge from Amazon, Indonesia, and the Democratic Republic of Congo (Hansen et al., 2013; Turubanova et al., 2018). However, the subsequent trend analyses may be affected by methodological changes. Specifically, the increased sensitivity of the change detection model after 2013 and improved detection of forest loss from 2015 onwards could lead to inconsistencies when comparing pre- and post-2013/2015 trends (Weisse and Potapov, 2021). This raises potential concerns about the accuracy of PF loss estimations derived from these datasets (Palahí et al., 2021).

Furthermore, those studies overlooked the resilience of PF, i.e., the ability of PF to recover to the pre-disturbance level in a short time (e.g., one year) with unchanged forest composition, structure, and ecosystem function (Seidl and Turner, 2022). They assumed PF that has undergone disturbance will directly convert to non-PF, such as SF or other land cover types. That could be true for PF impacted by severe disturbance, but not for PF that recovers quickly after mild disturbances. Furthermore, a comprehensive assessment of the long-term PF disparities between Haiti and the Dominican Republic is still unexplored. For instance, the disparities in PF conversion patterns (where PF changes to different land cover categories) and fragmentation levels have not been quantified. Additionally, the effectiveness of the designed protected areas in conserving PF, as well as the major drivers causing PF loss, have not been adequately studied. This has created difficulties in understanding PF disparities between the two countries and in providing support for biodiversity conservation policy in Haiti and the Dominican Republic.

To address these issues, this study has three major objectives: (1) to develop a time-series-based approach to detect PF with consideration of disturbance and resilience using dense Landsat time series; (2) to continuously map the land cover in Haiti and the Dominican Republic from 1996 to 2022 and quantify the PF conversion patterns; and (3) to compare the PF conservation status between Haiti and Dominican Republic and identify the major drivers of PF loss in Hispaniola. Through these objectives, this study aims to provide crucial data and insights to advance PF conservation efforts in Hispaniola. By integrating novel methodological approaches with an emphasis on PF resilience and the drivers of change, our findings contribute valuable knowledge to understanding and mitigating forest loss in this globally significant biodiversity hotspot.

2. Study area and datasets

2.1. Study area

The island of Hispaniola, located in the Caribbean region, has a

tropical climate. It is the second largest island in the Caribbean with an area of 76,192 km², after the island of Cuba (Fig. 1). Hispaniola is divided into two countries: Haiti on the western side covering an area of 27,750 km² and the Dominican Republic on the eastern side covering an area of 48,442 km². The topography of Hispaniola varies greatly, with elevations in Haiti ranging from -28 to 2678 m (mean \pm standard deviation, 408 \pm 373 m) and in the Dominican Republic from -58.0 to 3097 m (mean \pm standard deviation, 400 \pm 487 m).

Hispaniola has a rich biodiversity with a high level of endemism in many groups, including orchids, arthropods, amphibians, and reptiles (Fernández, 2007; Hedges et al., 2018; Sangermano et al., 2015b). However, the biodiversity faces significant human pressure due to the island's high population density, with over 11 million people in each country (Haiti and the Dominican Republic) in 2021 (UN, 2022). This demographic pressure poses a threat to local biodiversity and PF conservation.

Historical factors and economic disparities between Haiti and the Dominican Republic contribute to distinct pressure on PF conservation in the two countries (Marzelius and Droste, 2022). Haiti is regarded as the poorest country in the Western Hemisphere with a GDP per capita of around \$1,800 in 2022. Most of the economic activity in Haiti is centered around agriculture. In contrast, the Dominican Republic has the second largest economy in the Caribbean region with a GDP per capita of around \$10,000 in 2022. Tourism has replaced agriculture to become the largest contributor to the economy (Sangermano et al., 2015b).

2.2. Remote sensing and auxiliary dataset

We used all available Landsat Collection 2 Level 2 data to monitor land disturbances in Hispaniola. The Landsat data, spanning from January 1, 1984, to April 1, 2023, was downloaded from <https://earthexplorer.usgs.gov/> (access date: Apr 2023). However, due to the sparse data spanning from 1992 to 1995, we constrained our mapping period from 1996 to 2022. The dataset, comprising 5,780 images, covers eleven Landsat Worldwide Reference System (WRS)-2 scenes. We created the Landsat Analysis Ready Data for Hispaniola to facilitate analysis by projecting the original Landsat images to the Albers Equal Area coordinate system and clipping to predefined tiles.

Additionally, we compiled the 30-m resolution Shuttle Radar Topography Mission (SRTM) elevation data from <https://dwtkns.com/srtm30m/> (access date: Apr 2023). This dataset was used to calculate the slope and aspect for each pixel, aiding in land cover classification

and analysis of topographic characteristics in PFs. We also included 30-m Height Above the Nearest Drainage (HAND) data, which normalizes topography based on local relative heights within the nearest drainage network. This dataset provided insights into PF changes in relation to the topographic characteristics of the local environment (Donchyts et al., 2016; Heinrich et al., 2023; Nobre et al., 2011).

Furthermore, we obtained the protected area boundaries of Haiti and the Dominican Republic from the World Database on Protected Areas (WDPA) (UNEP-WCMC and IUCN, 2023). Our objective was to analyze the spatial distribution of PFs inside and outside protected areas. After close examination, we retained the major protected areas that contain the PF for further analysis (Fig. 1).

2.3. Training labels

We defined eight land cover types for Hispaniola, which include developed, primary wet forest, primary dry forest, secondary forest, shrub/grass, wetland, water, and other. Table 1 and Fig. A1 showed the descriptions of each land cover type and examples of high-resolution images, respectively. Through combining Google Earth high-resolution images, Landsat time-series and local expert knowledge, we collected high-quality training data with stable conditions. In total, we digitized 550 polygons, encompassing 342,013 pixels at 30-m resolution, between 2003 and 2022 (Table A1). The "Count of selected training sample" column means the number of pixels used to train the random forest classifier (see Section 3.1.2 for the details).

3. Methodology

The workflow for generating land cover (including PF) in Haiti and the Dominican Republic consists of three main components (Fig. 2). The first component is to prepare training data, which includes using the COLD (COntinuous monitoring of Land Disturbance) algorithm to detect land disturbance and extract temporal trajectory features (Zhu et al., 2020). The second component is to generate the land cover map with a random forest model, followed by post-processing steps. The third component is to evaluate the map's accuracy using the collected reference sample.

3.1. Land disturbance detection and cover classification

3.1.1. Land disturbance detection using all available Landsat data

We used the COLD algorithm to detect land disturbance and classify

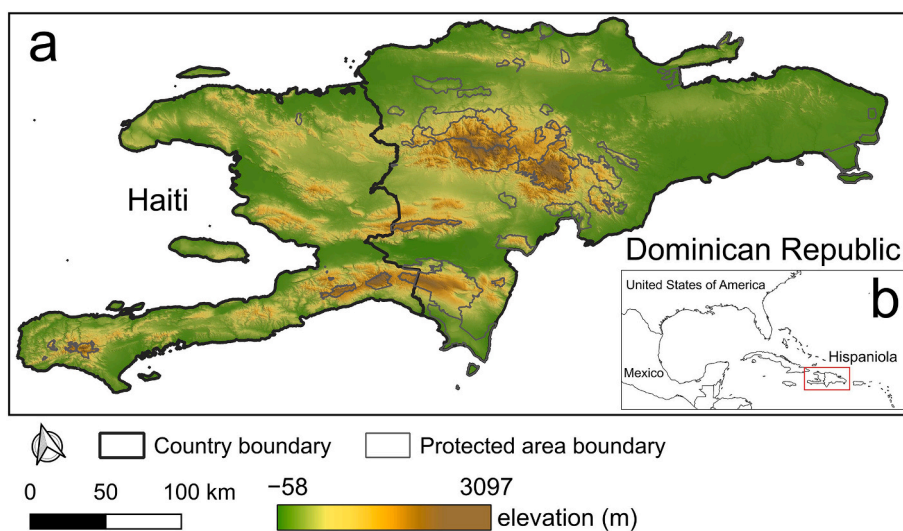


Fig. 1. Study area of Hispaniola. Inset (b) shows the location of Hispaniola. The background denotes elevation. The interior polygons denote the major protected area boundaries containing the primary forest in Haiti and the Dominican Republic, respectively.

Table 1
Standards when collecting training labels.

Land cover	Description
Developed	Land containing constructed materials with impervious surface percentages greater than 10%. Examples include roads, buildings, parking lots, and low-density residential.
Primary wet forest	A large patch of closed forest with nearly 100% tree cover. Primary wet forests are usually above 600 m in Hispaniola. The time series of forest change was considered when collecting the training sample of the primary wet forest. Primary wet forests should have abundant forest cover and have not undergone significant forest cover loss during the past four decades. The pristine and recovered primary wet forests are both collected.
Primary dry forest	A large patch of closed forest with nearly 100% tree cover. Primary dry forests are usually below 600 m in Hispaniola. The time series of forest change was considered when collecting primary dry forest as we did for primary wet forest.
Secondary forest	Areas with nonprimary forest tree cover greater than 10%, which include but are not limited to (1) degraded primary forests after significant natural disturbances, such as hurricanes and severe drought; (2) open forests after selective logging; (3) regrowth forests after clearance, such as regenerated forests from abandoned agricultural land; (4) tree plantations.
Shrub/Grass	Areas covered with naturally generated grassland, herbs, and bushes. The vegetation cover is greater than 10%, but usually, it is hard to identify any forest stands from high-resolution images.
Water	Areas with open water, generally with a water percentage greater than 50%. Examples include rivers, lakes, reservoirs, bays, and oceans.
Wetland	Areas where water saturation is the determining factor in soil characteristics and vegetation types. The soil or substrate is periodically saturated with or covered with water. A typical example in Hispaniola is mangrove forests.
Other	Areas not belonging to the land cover types defined above. It mainly consists of barren, croplands, and transitional types. Examples include cultivated crops, pasture for cattle, sand, rocks, bare soil, abandoned agricultural land with unnatural grassland, and deforested areas with shallow vegetation.

land cover with all available Landsat images from 1996 to 2022 (Zhu and Woodcock, 2014; Zhu et al., 2020). The COLD algorithm uses the combination of linear and harmonic models (Eq. (1)) to fit clear Landsat observations for each band, then dynamically compares the consequent clear observations with the model predictions. If the differences between a certain number of consecutive anomaly observations and model

predictions exceed the change probability, land disturbances are confirmed, and the corresponding temporal segment is created. When all the clear observations are processed, the extracted temporal trajectory parameters are used for land cover classification. Considering the relatively limited clear observations in Hispaniola and the fact that PF is sensitive to disturbance, we chose the sensitive parameter settings for the COLD algorithm by adjusting the number of consecutive anomaly observations from six (default) to four and change probability from 0.99 (default) to 0.95 (chi-squared distribution) (Zhu et al., 2020). More discussion is provided in Section 5.2.

$$\rho = a_0 + c_1x + a_1 \cos\left(\frac{2\pi}{T}x\right) + b_1 \sin\left(\frac{2\pi}{T}x\right) + a_2 \cos\left(\frac{2\pi}{T}x\right) + b_2 \sin\left(\frac{2\pi}{T}x\right) + a_3 \cos\left(\frac{2\pi}{T}x\right) + b_3 \sin\left(\frac{2\pi}{T}x\right) \quad (1)$$

where ρ is the surface reflectance from model prediction. T is the number of days per year (set to 365.25) and x is the Julian data. Parameter a_0 is the overall surface reflectance of the temporal segment. Parameter c_1 represents the inter-annual change (slope) for the temporal segment. Parameters $a_1, b_1, a_2, b_2, a_3, b_3$ are the coefficients for the harmonic functions.

3.1.2. Land cover classification based on COLD outputs

After running the COLD algorithm, we trained the random forest (RF) machine learning model to classify the land cover of each temporal segment. The predictor variables include the spectral-related parameters derived from COLD-fitted temporal segments and topographic characteristics (elevation, slope, and aspect) derived from the digital elevation model (Zhu and Woodcock, 2014). The RF model was selected since it has proven successful on large-scale classification tasks in previous research (Brown et al., 2020; Friedl et al., 2022).

The training sample distribution significantly affects the performance of the RF model (Belgiu and Drăguț, 2016; Zhu et al., 2016). Training sample with proportional distribution following the actual land cover map achieve better accuracy than training sample with equal distribution (Zhu et al., 2016). However, the proportion of each land cover in the training sample remains unknown without the wall-to-wall land cover map. To make the training sample proportion close to the actual distribution and achieve better accuracy, we first used the equal-

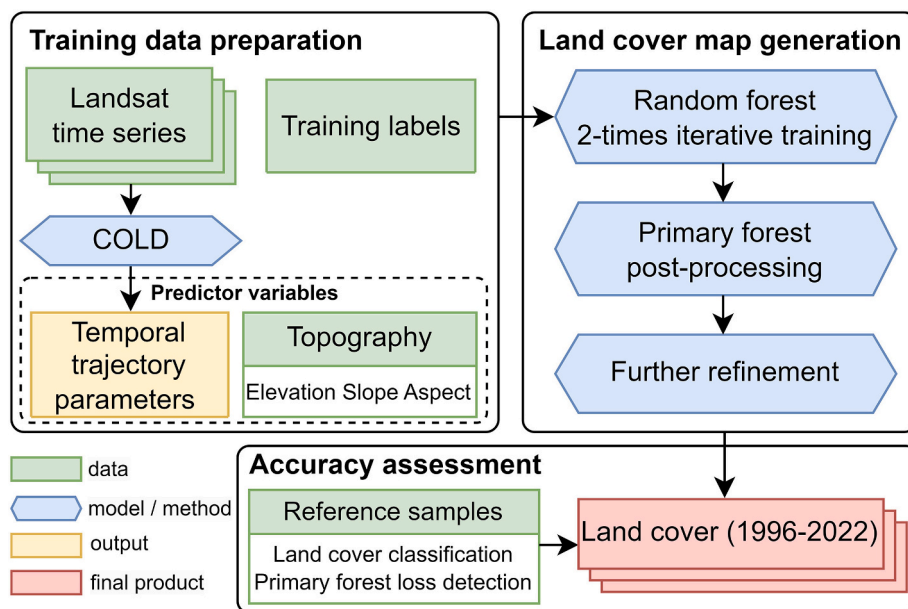


Fig. 2. Flowchart of land cover (including primary forest) map generation in Haiti and the Dominican Republic. COLD denotes the COtinuous monitoring of Land Disturbance algorithm (Zhu et al., 2020).

distribution training sample to generate the initial land cover classification to approximate the actual land cover proportion, and then adjusted the training sample proportion based on the proportion calculated from the initial results of land cover classification and the optimized strategy from [Zhu et al. \(2016\)](#). Around 25,000 sample points were randomly extracted from each digitized polygon to make sure each polygon contributed to the land cover classification. The number of training sample for each polygon was based on the polygon area. The final counts of selected training sample used for the RF training are provided in [Table A1](#).

3.1.3. Primary forest post-processing with the consideration of resilience and patch size

RF classification results contained errors that were not consistent with the real-world evolution of PF. For instance, PF which fully recovered to the pre-disturbance condition in a short time (recovered PF) was misclassified as SF. The degraded PF, which should have been classified as SF after disturbance, was still classified as PF. Additionally, regrowth SF was misclassified as PF. However, even in an ideal situation where seeds and stems of the original forest species are present, SF usually takes over 50 years to recover to PF ([Poorter et al., 2016](#)), which could not be observed during our mapping period (1996–2022). We also observed classification errors in the scattered PF pixels. Those scattered PF pixels, which are not large enough to support the biodiversity that PF normally supports, were misclassified as PF. To correct the classification errors, we applied three post-processing steps.

First, we separated the recovered PF and SF, which originate from degraded PF, by considering the resilience—specifically, whether the PF recovered shortly (e.g., one year) after the disturbance. We evaluated the condition of post-disturbance PF and calculated the corresponding vegetation index (VI) change before and after the disturbance. The VI change was calculated by subtracting the maximum vegetation index one year after the disturbance from the maximum vegetation index one year before the disturbance. We linked the short-term VI change to the PF recovery within a short time (one year) to indicate the resilience of PF in various disturbance agents.

To determine the optimal VI and threshold for assessing whether the post-disturbance PF had recovered, we randomly selected 120 potentially disturbed PF pixels from the initial land cover classification map in [Section 3.1.2](#). We scrutinized the Landsat time series and interpreted the disturbance agents. After excluding the 28 misclassified PF sample units, we selected five VIs and calculated the VI changes before and after the disturbance for the remaining 92 pixels and evaluated the PF condition after different disturbance agents. The details on the selected five VIs were provided in [Appendix B](#).

Among the selected VIs, we selected the Normalized Burn Ratio (NBR) ([Key and Benson, 2006](#)) index and 0.05 as the empirical threshold ([Fig. 3](#)). This threshold approximately separates PF disturbances induced by strong agents (fire, hurricane, landslide, and tree-cutting) and those induced by weak agents (such as drought) or commission error. We found that strong disturbance agents, such as fire, hurricanes, landslides, and tree-cutting, often lead to irreversible PF loss or degradation, converting PF into SF or other land cover types, and corresponding significant NBR declination. In contrast, the NBR change induced by drought is not as significant. The PF condition changes due to drought, such as loss of leaves, and can be detected by Landsat time series. However, the original PFs remain and recover to their pre-disturbance condition within a short time after the drought ends. This means that these PFs are resilient to drought. Furthermore, the NBR change caused by drought is similar in magnitude to that caused by commission errors of the change detection algorithm. This suggests that including the PF loss induced by drought or other recoverable disturbances may introduce considerable commission errors of PF loss detection.

Compared to NBR, it is challenging to find a single threshold among other VIs that can separate the degraded PF experiencing strong

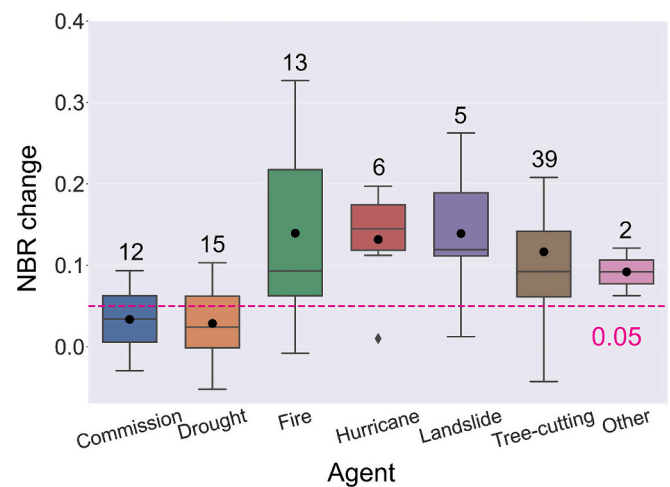


Fig. 3. Boxplots showing Normalized Burn Ratio (NBR) index changes for different primary forest disturbance agents, which are calculated by subtracting post-disturbance NBR from pre-disturbance NBR. The numbers on top of the boxplots indicate the sample count for each agent. In each boxplot, the dot and line inside the boxplot represent the mean and median values, respectively. The box of the boxplot represents the interquartile range (the range between the first and third quartiles). The whiskers represent the maximum and minimum values of the plot data within 1.5 times of the interquartile range from the first and third quartiles, respectively. The diamond point represent outliers that fall outside the whiskers.

disturbances from recovered PF experiencing weak disturbances ([Fig. B1](#) in [Appendix B](#)). Although NBR is designed to enhance the burned area, previous studies have demonstrated its usefulness in indicating forest recovery and resilience ([Cohen et al., 2018](#); [Kennedy et al., 2012](#); [White et al., 2017](#)).

Therefore, for PF pixels that experienced disturbance, if the absolute NBR change (Δ NBR) did not exceed 0.05 one-year after the disturbance, the post-disturbance segment remained as PF ([Fig. 4a](#)). If the absolute NBR change exceeded 0.05 and the post-disturbance segment was classified as PF, we corrected it to SF ([Fig. 4b](#)).

Second, we corrected the PF classification results for segments that previously contained non-PF classifications, reclassifying them as SF ([Fig. 4c](#)). If previous segments were classified as non-PF types, but the current segment was classified as PF, we corrected the current segment to SF. This was to correct the errors of misclassifying growing SF as PF. Third, we defined the 3×3 minimum mapping unit (MMU) for PF clusters to exclude the misclassified scattered PF pixels. To achieve this, we segmented the PF pixels into multiple clusters based on the 8-neighbor rule and converted the PF clusters that do not contain the 3×3 PF structure to SF. The reason we selected 3×3 as the MMU is that the central pixel surrounded by neighboring PF pixels is less affected by the impact of edge effects ([Laurance et al., 1997](#)). It can serve as the core habitat for the connected PF pixels. The line-shape PF clusters do not include the core habitat to support biodiversity and were thus removed.

3.1.4. Further refinement of the land cover map

After reducing errors in PF classification, we made further refinements to improve the land cover map based on the time series trajectory. First, we corrected the misclassified developed pixels. For temporal segments classified as developed but with subsequent segments consistently classified as non-developed, we replaced the segment that was classified as developed (first segment in [Fig. 4d](#)) with the land cover type associated with the second highest prediction probability in the RF model.

Second, we filled the gaps in the land cover time series to ensure the continuity of land cover from 1996 to 2022. Data density issues can affect the initialization and fitting of the COLM algorithm, leading to

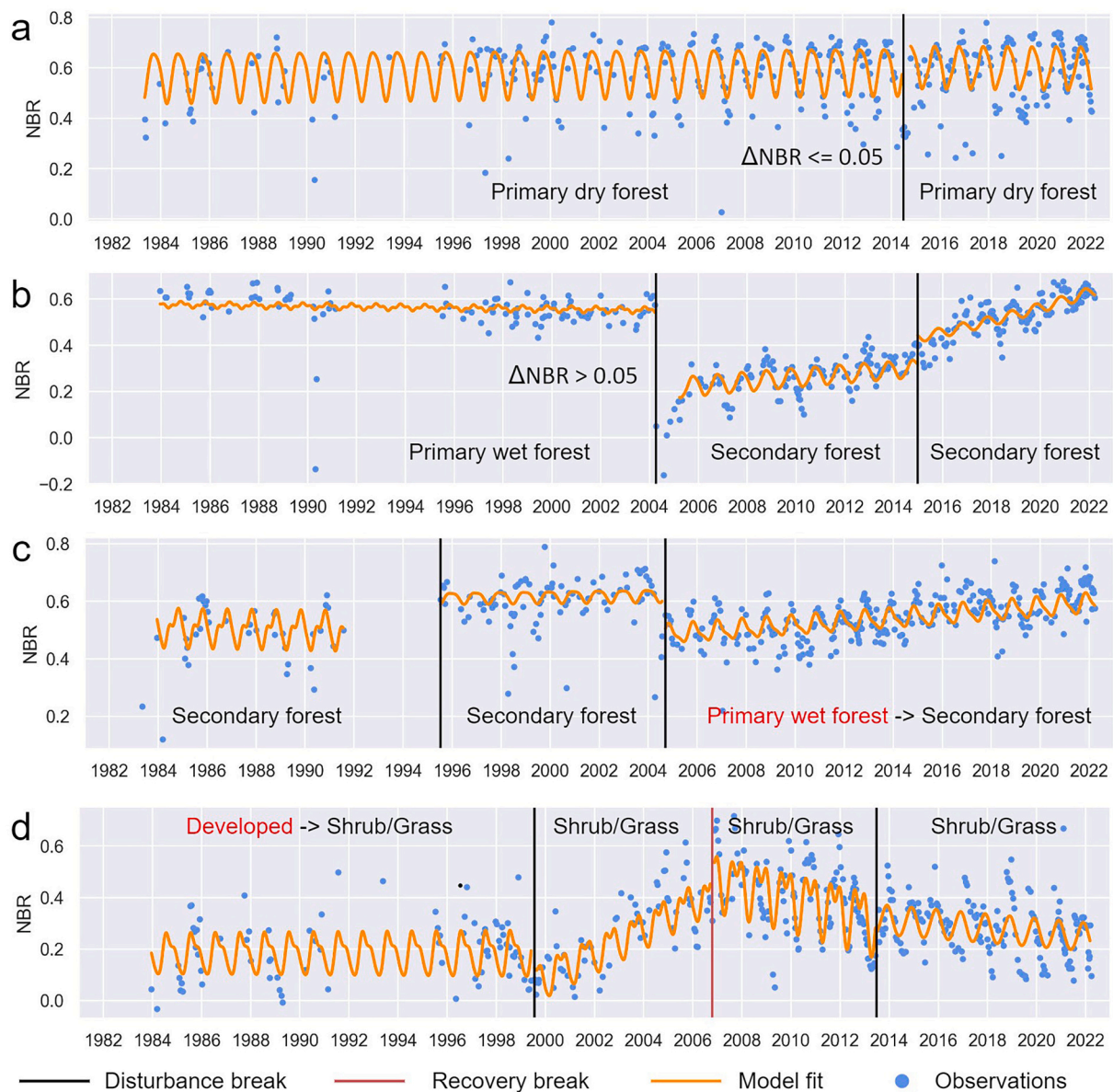


Fig. 4. Schematic of post-processing steps. Subplots (a) and (b) display the time series of the Normalized Burn Ratio (NBR) index at (17.56609 N, 71.51920 W) and (19.02904 N, 70.97138 W), respectively. Those pixels experienced drought (a) and fire (b), respectively. Subplots (a) and (b) illustrate the process of separating recovered primary forest (PF) and secondary forest using the NBR threshold. Subplot (c) displays the time series of the NBR index at (19.00815 N, 71.18575 W). It shows the process of correcting the misclassified PF whose previous segments were classified as non-PF. The red text shows the misclassified results from the random forest model. Subplot (d) displays the time series of the NBR index at (18.28849 N, 71.34908 W). It shows the process of correcting the misclassified developed pixels whose subsequent segments were classified as non-developed types. (For interpretation of the references to colour in this figure legend, the reader is referred to the web version of this article.)

gaps in the land cover time series (Zhang et al., 2022). To address this issue, we used subsequent land cover segments to fill these gaps. If the land cover remained discontinuous at the end with no subsequent segments available, we extended the previous classification segments to fill the gaps.

3.2. Accuracy assessment and primary forest loss driver identification

We used two sets of stratified random samples to evaluate the land cover classification accuracy and PF loss detection accuracy. The spatial unit is the mapped Landsat pixel (30 m × 30 m). When interpreting PF loss sample, we also recorded the drivers causing PF loss to determine the major drivers contributing to PF loss in Hispaniola.

For the accuracy assessment of land cover classification, we followed

the good practice workflow to generate and allocate the reference sample (Olofsson et al., 2014). We set the target standard error of the estimated overall accuracy as 0.02 and conjectured the user's accuracies as 0.8 for all types. The total sample size is 400 (Eq. 13 in Olofsson et al. (2014)). The stratum weight was calculated based on 27-year land cover maps. For rare classes (less than 10%), fifty sample units were allocated for primary wet and dry forests stratum to reduce the estimated variance. Twenty-five sample units were allocated to other rare strata. The remaining reference sample was allocated proportionally to the dominant stratum (more than 10%).

Four trained interpreters were involved in the interpretation. To reduce the interpreter's variability in the understanding of each land cover, four interpreters interpreted the 40 mutual sample units (5 random sample units from each stratum) as the training before the

formal interpretation. When interpreting reference sample, four interpreters had no prior information about the reference sample (i.e., “blind” interpretation) and interpreted the reference sample independently. Google Earth high-resolution images, Landsat time series observations, and elevation information were used together to label the reference sample. The dominant land cover type with the largest proportion was assigned as the label for the reference sample. After completing the interpretation of 40 mutual sample units, four interpreters convened to discuss the scoring criteria and reached a final decision on the sample units with disagreement. In this way, we ensured the understanding of each stratum is consistent among different interpreters to reduce interpreter variability (Olofsson et al., 2014; Pengra et al., 2020; Powell et al., 2004).

After completing the interpretation of the 40 mutual sample units, four interpreters were assigned to interpret the remaining sample. In addition to labeling the land cover types, each interpreter also recorded the confidence levels (100%, 80%, 50%, or less than 50%) for each reference sample. After completing the initial interpretation, all interpreters re-interpreted challenging sample with low confidence level (50% or less). The final labels of these challenging sample units were determined using majority vote and group discussion. We excluded reference sample where interpreters could not reach an agreement and sample that lacked reliable reference sources, such as sample with dynamic and mixed land cover before 2000. The excluded sample units were approved by all interpreters.

After finishing the interpretation, we reported the user’s accuracy, producer’s accuracy, overall accuracy, and the uncertainties at the 95% confidence level based on agreement between the reference label and mapped land cover type (Olofsson et al., 2014). The agreement was defined as the exact match between the reference label and mapped type.

For the accuracy assessment of PF loss detection, we defined two strata: PF loss and other. These were based on the accumulated PF loss map spanning the entire period from 1996 to 2022. PF loss indicates that a pixel was classified as PF in 1996 but changed to non-PF types between 1996 and 2022. The other stratum refers to pixels that remained stable PF from 1996 to 2022 or were classified as other non-PF land cover types. We followed the same workflow of the land cover classification assessment to assess the accuracy of PF loss detection. We generated 486 sample units by setting the standard error of the estimated overall accuracy as 0.01 and conjecturing the user’s accuracy of PF loss and other as 0.7 and 0.95. We assigned 100 and 386 sample units for the PF loss and other strata, respectively. If the reference sample is labeled as PF loss, we also recorded the driver of PF loss. We listed five major drivers of PF loss in Hispaniola based on prior information, which includes fire, tree-cutting, hurricane, landslide, and other. Like the process of labeling reference sample, we identified the drivers of PF loss using multi-source information (including Google Earth high-resolution images, Landsat time series observations, etc.) and group discussions from all interpreters.

3.3. Spatiotemporal comparison of primary forest status between Haiti and the Dominican Republic

After generating the land cover dataset that distinguishes PFs and SFs in Hispaniola, we conducted a spatiotemporal comparison of the PF status in Haiti and the Dominican Republic to evaluate PF conservation status. We quantified the annual PF loss rate, identified hotspots of PF loss, and determined the major drivers causing the hotspots of PF loss. We also compared the PF changes inside and outside protected areas in both countries to explore the effectiveness of protection policy on PF.

The topographic characteristics of PF were also analyzed to explore the factors affecting PF loss. We investigated the distribution of existing and lost primary wet and dry forests across the elevation and slope gradients and calculated changes in mean elevation and slope of PFs from 1996 to 2022 using SRTM and HAND datasets. Additionally, we

evaluated the fragmentation level of PFs by calculating the patch density (number of PF patches per 100 km²) and mean patch area of PFs. We segmented the PF pixels into distinct patches based on the 8-neighbor rule, then computed the number of PF patches, patch density, and mean patch area for Haiti and the Dominican Republic. A sparse distribution of PF patches with smaller average patch sizes indicates higher levels of forest fragmentation, and vice versa. These analyses comprehensively demonstrate the PF disparity between Haiti and the Dominican Republic.

4. Results

4.1. Annual land cover change in Haiti and the Dominican Republic

We generated the annual 30-m land cover map from 1996 to 2022 and determined rates of PF loss (Fig. 5). Fig. 5 shows that Haiti has less PF (including the primary wet and dry forests) coverage and a higher proportion of PF loss compared to the Dominican Republic. The map-based analysis reveals that PF in Haiti decreased from 20,447 ha (0.75%) to 12,023 ha (0.44%) with a decrease rate of 324 ha/y. The total area of PF decreased by 41.2% from 1996 to 2022 (Fig. 6). The findings align with the previous study by Hedges et al. (2018) which also reported less than 1% PF coverage in Haiti. In contrast, PF (including the primary wet and dry forests) in the Dominican Republic decreased from 343,221 ha (7.14%) to 272,913 ha (5.67%) with a decrease rate of 2,704 ha/y. The total area of PF decreased by 20.5 % from 1996 to 2022.

The map-based annual land cover change results show that the developed area in Haiti increased from 0.63% (~21,068 ha) to 1.32% (~44,095 ha) with an expansion rate of ~717 ha/year (Fig. 6). In contrast, the developed area of the Dominican Republic increased from 1.37% (~81,101 ha) to 1.96% (~116,119 ha) with an expansion rate of ~1,090 ha/year.

Not surprisingly, the proportion of SF increased in both countries due to the strong disturbance of PF, which often leads to SF formation, and the growth of SF from abandoned cropland and deforested areas. One of the most surprising results is that more than half of the land surface in Haiti is covered with barren, abandoned cropland, or deforested surface (“other” type with gray line in Fig. 6), a much higher proportion than in the Dominican Republic. This is likely due to intensive and successive agricultural activities and deforestation in the 20th century (see the Discussion section for details) (Cohen, 1984; Hedges et al., 2018; Marzelius and Droste, 2022).

We also analyzed the PF conversion pattern in Haiti and the Dominican Republic (Fig. 7). Map-based results show that Haiti experienced the largest PF loss during the 2016–2017 period, which was mainly caused by Hurricane Matthew (refer to Section 4.3 for more details). Around 78.4% of lost PF converted to SF when disturbances occurred, while around 21.6% of lost PF converted to other land cover types. In contrast, in the Dominican Republic, around 91.3% of lost PF transitioned to SF, and around 8.7% of lost PF converted to other land cover types (Fig. 7). The mapping results show that both Haiti and the Dominican Republic have experienced substantial PF loss, with the situation in Haiti being worse than that in the Dominican Republic.

4.2. Map accuracy and major primary forest loss drivers

For the accuracy assessment of land cover classification, we excluded 29 sample units that are difficult to label (Table C1). The area-based confusion matrix shows that the overall accuracy of land cover classification is 80.5% (±5.2%) [95% confidence interval] (Table 2). Specifically, the user’s and producer’s accuracies for primary wet forest classification are 83.7% (±10.5%) and 84.4% (±25.2%), respectively. The user’s and producer’s accuracies for primary dry forest classification are 86.0% (±9.7%) and 96.0% (±7.6%), respectively. The large variances are attributed to the limited number of reference sample and the mixture with large proportion types, such as SF. The area adjustment

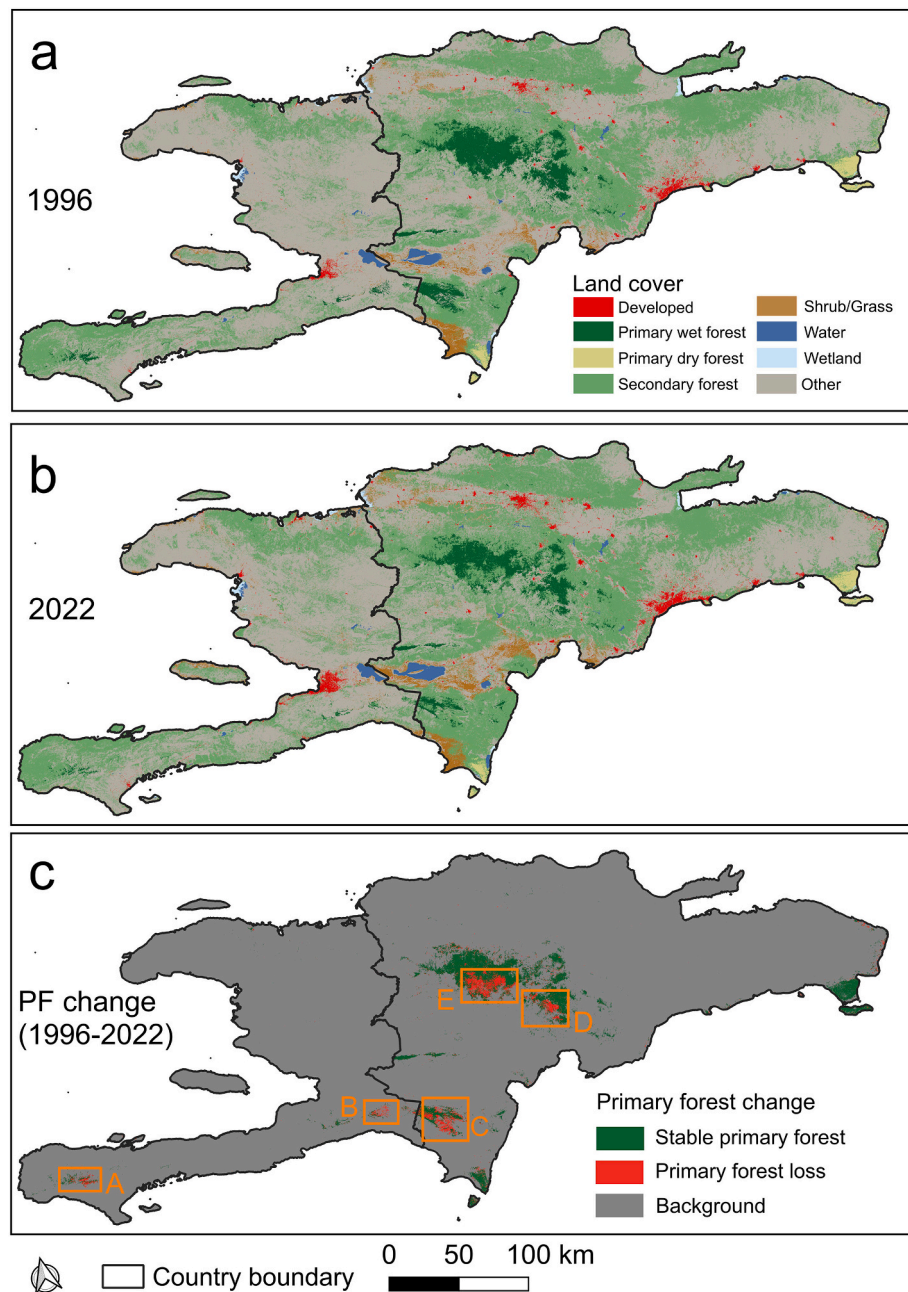


Fig. 5. Land cover maps of Hispaniola in 1996 (a) and 2022 (b). Subplot (c) shows the primary forest (PF) change information. The five rectangles in subplot (c) are the hotspots of primary forest loss enlarged in Fig. 8.

results show that both primary wet and dry forests are slightly overestimated based on the current land cover map, suggesting that there is less remaining PF in Hispaniola. Shrub/Grass has the lowest accuracy with the user's and producer's accuracies of 39.1% ($\pm 20.4\%$) and 23.4% ($\pm 17.0\%$), respectively. This is because (1) the spectral signature of shrub/grass is frequently mixed with SF and other types; (2) shrub/grass is a rare type with the mapped proportion of 2.4%. Their accuracies can be significantly affected by dominant types, such as SF and other types.

For the accuracy assessment of PF loss detection, we excluded six hard-to-interpret sample units (Table C2). The area-based confusion matrix shows that the overall accuracy is 99.4% ($\pm 0.5\%$) (Table 3). The user's and producer's accuracies for PF loss detection are 68.8% ($\pm 9.3\%$) and 73.6% ($\pm 38\%$), respectively. The large variance in the producer's accuracy is due to the significant area difference between the PF loss stratum (1.05%) and the other stratum (98.95%) (Olofsson et al.,

2020). The area adjustment result shows that the current map slightly overestimates the PF loss area with a bias of 52.3 km² (Table 3).

The PF loss driver analysis based on the sample interpretation shows that fire (44/67) accounts for 65.7% PF loss in Hispaniola, equivalent to 482.7 km². Tree-cutting (14/67) caused 20.9% PF loss, equivalent to 153.6 km². Hurricanes (9/67) caused 9.0% PF loss, equivalent to 65.8 km². Landslides (2/67) caused 3.0% PF loss, equivalent to 21.9 km². Though PFs are resilient and could sustain many of the wildfires if they are not severe enough, fires still contribute almost two-thirds of total PF loss.

4.3. Hotspots of primary forest loss

We further explored the hotspots of PF loss highlighted in Fig. 5c and displayed the PF loss year (Fig. 8). In hotspot A near the Grande Colline

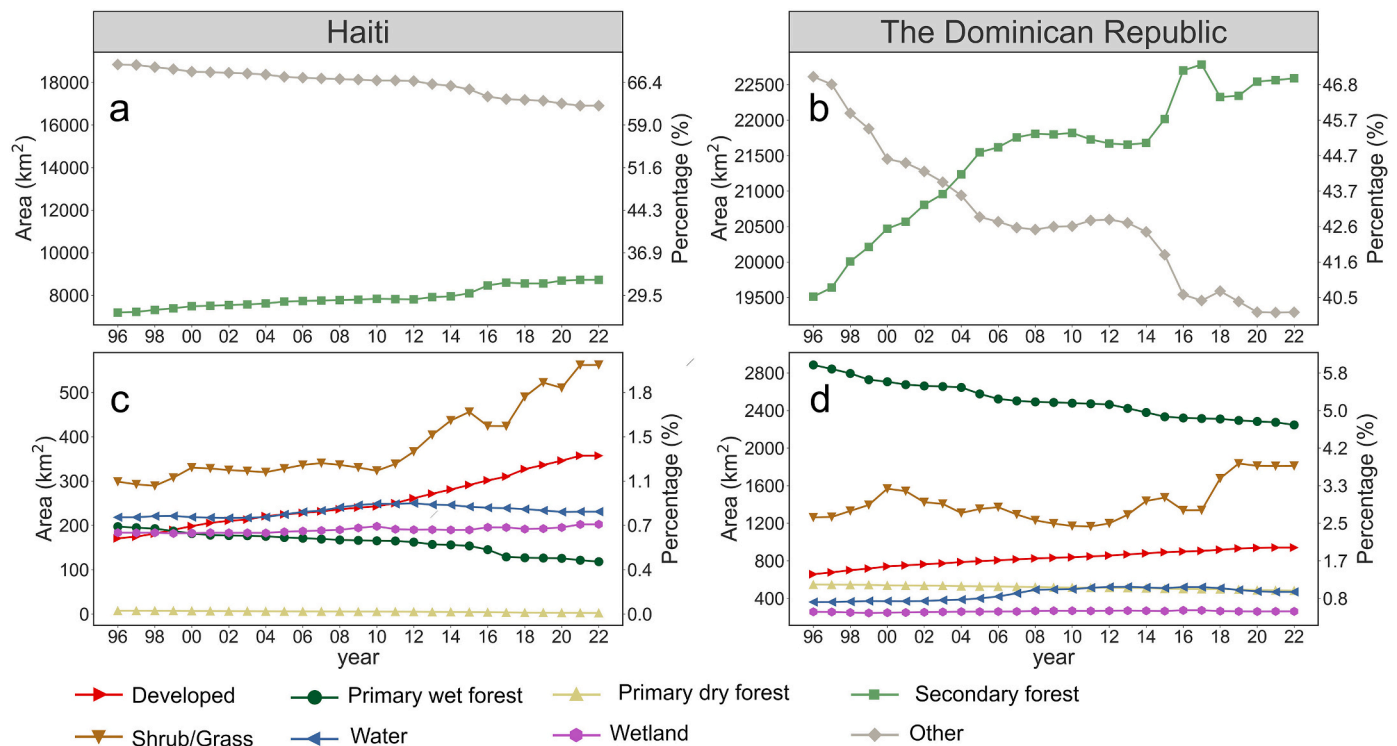


Fig. 6. Map-based land cover change in Haiti (a & c) and the Dominican Republic (b & d) from 1996 to 2022. The left and right y-axes show the area and corresponding percentage, respectively. For better visualization, the curves for secondary forest and other land cover types are displayed separately due to the significantly unbalanced proportions among the various land cover types.

National Park and Macaya National Park in Haiti (Fig. 8), most of the PF loss happened during 2016 and 2017. This was mainly caused by Hurricane Matthew in Oct 2016, which caused widespread destruction of housing, affecting 2.1 million people, and causing over 500 deaths in that country (De Giorgi et al., 2021). Because of the availability of Landsat data and cloud cover impact, confirmation of some PF loss that happened during this event was delayed until the availability of clear Landsat data as late as 2017. Besides the PF loss from Hurricane Matthew, we found that subsequent PF loss in 2021 and 2022 in the same affected region, corresponded to landslides caused by the 2021 Haiti Earthquake. The earthquake resulted in many large landslides that destroyed PF. The 14 August 2021 earthquake is considered the largest natural disaster on Earth for that year, causing 2,250 fatalities, and climatic preconditioning from Hurricane Matthew exacerbated the slope instability leading to landslides (Havenith et al., 2022).

We further plotted the land cover change in Macaya National Park (Fig. 9), which is the largest national park in Haiti with the highest proportion of PF. Map-based results show that Hurricane Matthew in 2016 and the Earthquake in 2021 caused 1,910 ha and 411 ha of PF loss in Macaya National Park, respectively. These losses account for 22.6% and 4.9% of the total PF loss area in Haiti between 1996 and 2022 (8,424 ha based on Fig. 6). Moreover, based on the PF areas in Haiti in 2015 (15,785 ha) and 2020 (12,823 ha), the PF losses in Macaya National Park caused by Hurricane Matthew in 2016 and the Earthquake in 2021 represent 12.10% and 3.21% of the national PF area, respectively. Additionally, landslides in 2021 caused significant SF loss (~294 ha) and expansion of barren land in Macaya National Park (Fig. 9).

Hotspot B near the Forêt de Pins region in Haiti shows a more fragmented PF loss pattern. This region experienced dramatic deforestation during the 20th century and the pattern of existing PF in 1996 was already fragmented. Continuous human pressure resulted in ongoing PF loss, reflecting a fragmented and vulnerable forest landscape.

Hotspot C near the Sierra de Bahoruco National Park in the Dominican Republic, shows multiple large patches of PF loss in a single year.

Map-based results show the areas of PF loss in 2000, 2007, 2013, 2015, and 2022 were around 838 ha, 1,109 ha, 3,265 ha, 1,245 ha, and 2,242 ha, respectively. Landsat time series confirmed fire is the major driver causing the PF loss in these years.

Hotspot D near the Valle Nuevo National Park in the Dominican Republic shows two large patches of PF loss that occurred in 2014 and 2015, which was due to the fire in the summer of 2014. Map-based results show around 5,000 ha of PF loss, which accounted for about 1.76% of the Dominican Republic's total PF in 2014.

Hotspot E near the José del Carmen Ramírez National Park in the Dominican Republic shows two big fire events in 1997 and 2005, accounting for the major PF loss events. Map-based results show a loss of approximately 6,400 ha and 10,900 ha PF in 1997 and 2005, respectively. These losses accounted for about 1.9% and 3.4% of the total PF in the Dominican Republic in the respective years.

4.4. Primary forest change within and outside the protected area

We compared the distribution and variation of PF within and outside the protected areas in Haiti and the Dominican Republic (Fig. 10). Map-based results show that approximately 31% of primary forests in Haiti are not within protected areas. This is particularly notable for primary dry forests, with about 50% located outside protected areas. In contrast, the Dominican Republic has 86% of its PFs contained within protected areas, which aligns with expectations given its larger number of designated protected areas.

In Haiti, PF loss inside the protected area covers a higher proportion of the total primary forest loss for both primary wet and dry forests. Not only is the area of PF loss greater inside these areas, but the proportion of total PF loss is also higher. In the Dominican Republic, the loss of primary wet forest inside protected areas accounts for the majority of the total primary wet forest loss. However, the loss of primary dry forest outside protected areas constitutes the majority of total primary dry forest loss. This is because most of the primary dry forest is well-

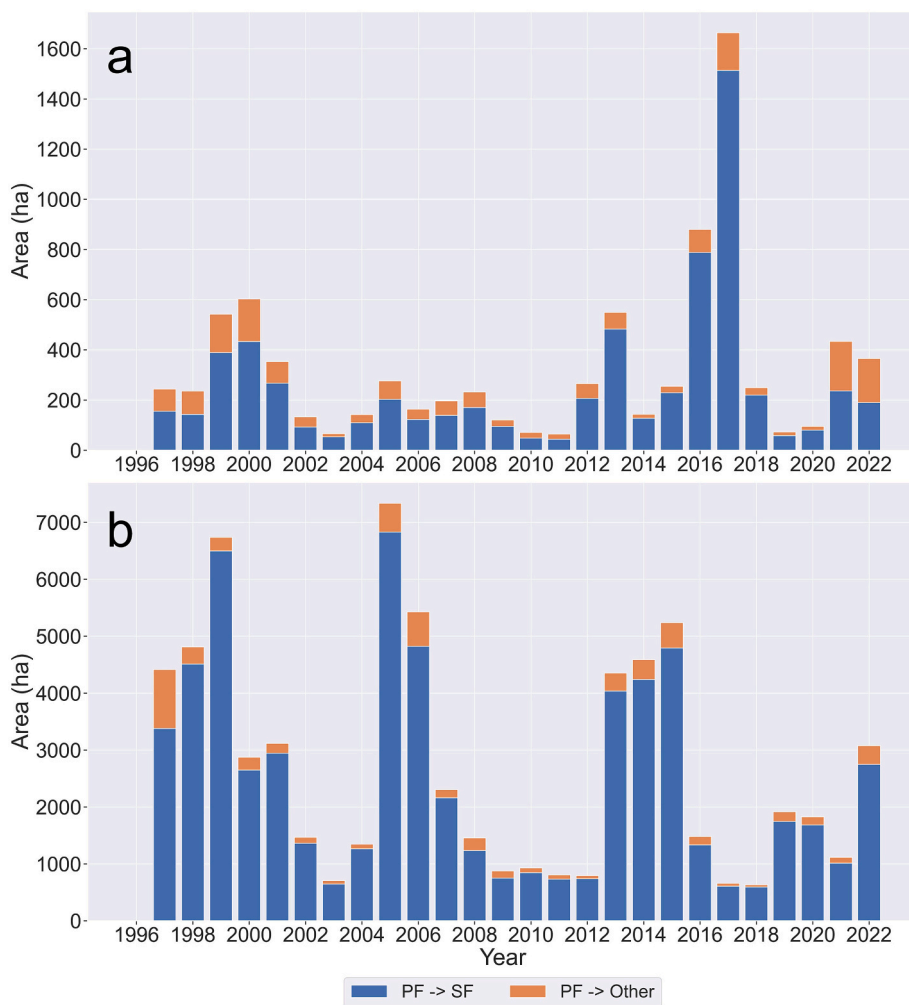


Fig. 7. Map-based annual loss and conversion of primary forest (PF, including primary wet and dry forests) from 1996 to 2022 in Haiti (a) and the Dominican Republic (b), respectively. Each value for a given year indicates the detected PF loss area from the previous year to the indicated year. For example, the value for the year 2022 indicates the detected PF loss area from 2021 to 2022. The blue colour represents the area of PF converted to secondary forest (SF), while the orange colour represents the area of PF converted to other land cover types. (For interpretation of the references to colour in this figure legend, the reader is referred to the web version of this article.)

preserved in Jaragua National Park and Cotubanamá National Park in the southern Dominican Republic.

4.5. Topographic characteristics of primary forest

We analyzed the topographic characteristics of the primary wet and dry forests in Hispaniola (Fig. 11). There is a notable elevation distinction between primary wet and dry forests. Most primary dry forests are in low-elevation areas (typically below 600 m) with small slope (typically less than 5 degrees). In contrast, most primary wet forests are in high-elevation areas (typically above 600 m). In Haiti, primary wet forests are concentrated in two zones: Zone I is around 1,500 m with a slope of ~40 degrees while Zone II is around 2,000 m with a slope of ~10 degrees (Fig. 11a). In the Dominican Republic, the primary wet forests are concentrated in regions with elevations ranging from 1,100 to 2,100 m and the slope ranges from 5 to 35 degrees (Fig. 11c).

We also analyzed topographic characteristics of the lost primary wet forest to explore factors affecting its loss. Fig. 11b shows that most of the primary wet forest loss happened in Zone II, indicating that regions with lower slopes are more prone to primary wet forest loss. This phenomenon is also observed in the Dominican Republic. Fig. 11d shows a relatively high proportion of primary wet forest loss in relatively small-slope regions. To study it in detail, we analyzed the mean elevation and slope

change of primary wet forests from 1996 to 2022 using the SRTM and HAND topography datasets (Fig. 12). Our analysis revealed that, in general, the mean SRTM elevation of primary wet forests is decreasing while the mean HAND elevation of them is increasing. Additionally, the mean slope of primary wet forests in Haiti and the Dominican Republic shows increasing trends in both datasets.

The slope change is as predicted: primary wet forest has a higher probability of surviving on land with steeper slopes because it is more inaccessible to humans. This implies that slope emerges as an important factor of PF loss. The mean slope declination in Haiti after 2020 is attributed to landslide-induced PF loss, which is the major contributor to PF loss, as PF in steeper regions is more likely to be affected by landslide (Havenith et al., 2022). This further implies that slope plays a critical role in affecting PF loss. The decrease in SRTM elevation (120 m in Haiti and 40 m in the Dominican Republic) is because PF in higher elevations but with relatively smaller slope has a greater contribution to the PF loss. The increase in HAND elevation suggests that PFs closer to a drainage basin are more susceptible to disturbances from human activities and natural events, such as hurricanes (Heinrich et al., 2023).

4.6. Primary forest fragmentation in Haiti and the Dominican Republic

Fragmentation analysis of PFs shows that Haiti has a lower patch

Table 2

Confusion matrix of land cover classification in area proportions, adjusted area, and reported accuracy at the 95% confidence interval. The “Map bias” denotes the mapped area minus the adjusted area. The “Area 95% CI” denotes the uncertainty of the adjusted area at the 95% confidence interval.

Map	Reference								
	Developed	Primary wet forest	Primary dry forest	Secondary forest	Shrub/Grass	Water	Wetland	Other	Total
Confusion matrix, area proportion									
Developed	0.0116	0	0	0.0007	0	0	0	0.0021	0.014
Primary wet forest	0	0.0297	0	0.0058	0	0	0	0	0.036
Primary dry forest	0	0.0001	0.0060	0.0008	0	0	0	0	0.007
Secondary forest	0	0.0054	0.	0.3052	0.0161	0	0	0.0643	0.391
Shrub/Grass	0	0	0	0.0104	0.0094	0	0	0.0042	0.024
Water	0	0	0	0	0	0.0083	0.0004	0.0004	0.009
Wetland	0	0	0.0003	0.0008	0	0.0010	0.0040	0	0.006
Other	0	0	0	0.0581	0.0145	0	0.0097	0.4310	0.513
Total	0.012	0.035	0.006	0.382	0.040	0.009	0.014	0.502	
Area and accuracy									
Mapped area (km ²)	29,149.5	72,126.7	14,133.7	793,648.0	48,599.4	18,402.4	12,176.6	1,042,143.2	
Adjusted area (km ²)	23,597.2	71,505.4	12,662.4	775,188.3	81,127.4	18,959.6	28,516.9	1,018,822.0	
Map bias (km ²)	5,552.3	621.2	1,471.4	18,459.6	-32,528.1	-557.2	-16,340.3	23,321.1	
Area 95% CI (km ²)	5,016.6	22,610.9	1,695.4	99,552.2	50,153.4	2,725.6	27,261.0	100,241.3	
User’s accuracy (%)	81.0 ± 17.2	83.7 ± 10.5	86.0 ± 9.7	78.1 ± 9.3	39.1 ± 20.4	92.0 ± 10.9	66.7 ± 19.3	84.0 ± 7.0	
Producer’s accuracy (%)	100.0 ± 0.0	84.4 ± 25.2	96.0 ± 7.6	79.9 ± 6.9	23.4 ± 17.0	89.3 ± 8.8	28.5 ± 27.7	85.9 ± 5.9	
Overall accuracy (%)	80.5 ± 5.2								

Table 3

Confusion matrix of primary forest (PF) loss detection in area proportions, adjusted area, and reported accuracy at the 95% confidence interval. The “Map bias” denotes the mapped area minus the adjusted area. The “Area 95% CI” denotes the uncertainty of the adjusted area at the 95% confidence interval.

Map	Reference		
	Other	PF loss	Total
Confusion matrix, area proportion			
Other	0.9870	0.0026	0.9895
PF loss	0.0033	0.0072	0.0105
Total	0.9902	0.0098	
Area and accuracy			
Mapped area (km ²)	74,411.9	787.3	
Adjusted area (km ²)	74,464.2	735.1	
Map bias	-52.3	52.3	
Area 95% CI (km ²)	386.8	386.8	
User’s accuracy (%)	99.7 ± 0.5	68.8 ± 9.3	
Producer’s accuracy (%)	99.7 ± 1.0	73.6 ± 38	
Overall accuracy (%)	99.4 ± 0.5		

density than the Dominican Republic (blue lines in Fig. 13). Additionally, the mean patch area of PF (orange lines in Fig. 13) in Haiti is smaller than that of the Dominican Republic, for both primary wet and dry forests. Those findings indicate a higher level of PF fragmentation in Haiti.

The patch density of primary wet forest in Haiti generally decreased due to the ongoing human pressure from tree-cutting (Fig. 13a). There was a sudden increase in the patch density of primary wet forests from 2016 to 2017, caused by the fragmentation of large PF patches in Macaya National Park induced by Hurricane Matthew. The mean patch area of the primary wet forest decreased consistently with fragmentation. For primary dry forests in Haiti, the time series of the fragmentation level change showed that the patch density and mean patch area decreased from 1996 to 2022, indicating simultaneous clearance of small primary dry forest patches and fragmentation of large primary dry forest patches (Fig. 13b).

In the Dominican Republic, the mean patch area of primary wet forest consistently decreased, while the patch density initially increased and then decreased after peaking in 2014 (Fig. 13c). This implies that the primary wet forest loss was initially dominated by the fragmentation

of large-patch primary wet forest into small patches. Subsequently, the patch density was reduced by the clearance of small patches of primary wet forest. The primary dry forest shows a different pattern compared with the primary wet forest (Fig. 13d). The patch density decreased with the increase in the mean patch area. This indicates that small patches of primary dry forest were removed while the large patches were not, corresponding to the primary dry forest in Jaragua National Park and Cotubanamá National Park, the two largest areas of primary dry forest in the Dominican Republic.

The ongoing PF fragmentation in Haiti and the Dominican Republic exacerbates edge effects, further encroaching on the remaining PFs (Laurance et al., 1997). This fragmentation also impedes forest recovery, as the growing distance between PFs and SFs limits natural regeneration process (Heinrich et al., 2023). Moreover, the higher level of PF fragmentation in Haiti poses significant challenges for maintaining biodiversity. Smaller and less connected habitats increase the risk of biodiversity loss, further threatening ecological stability (Hedges et al., 2018).

5. Discussion

5.1. Implications of primary forest mapping in Hispaniola

Primary forest is critical habitat for supporting biodiversity in tropical regions (Gibson et al., 2011). Separating PF and SF is therefore critical for evaluating the true impact of forest loss on biodiversity. Our study successfully distinguished PF and SF using dense Landsat time series data and high-quality training sample. We developed a quantitative and standardized approach for continuously mapping PF and SF, which can potentially be used to create a universal PF and SF map on a large scale. Factors such as forest height and age may be considered for inclusion in future mapping efforts.

When mapping PF, we considered its resilience, defined as the ability of PF to recover to pre-disturbance levels within a short period (e.g., one year) with unchanged forest composition, structure, and ecosystem function (Seidl and Turner, 2022). We measured PF recovery and indicated the resilience using changes in vegetation indices (VIs) before and after the disturbance. Through sample interpretation (Sections 3.1.3), we used the change in NBR index with a threshold of 0.05 to distinguish PF that has quickly recovered within one year after a weak disturbance and PF that has been permanently degraded and converted to SF after a

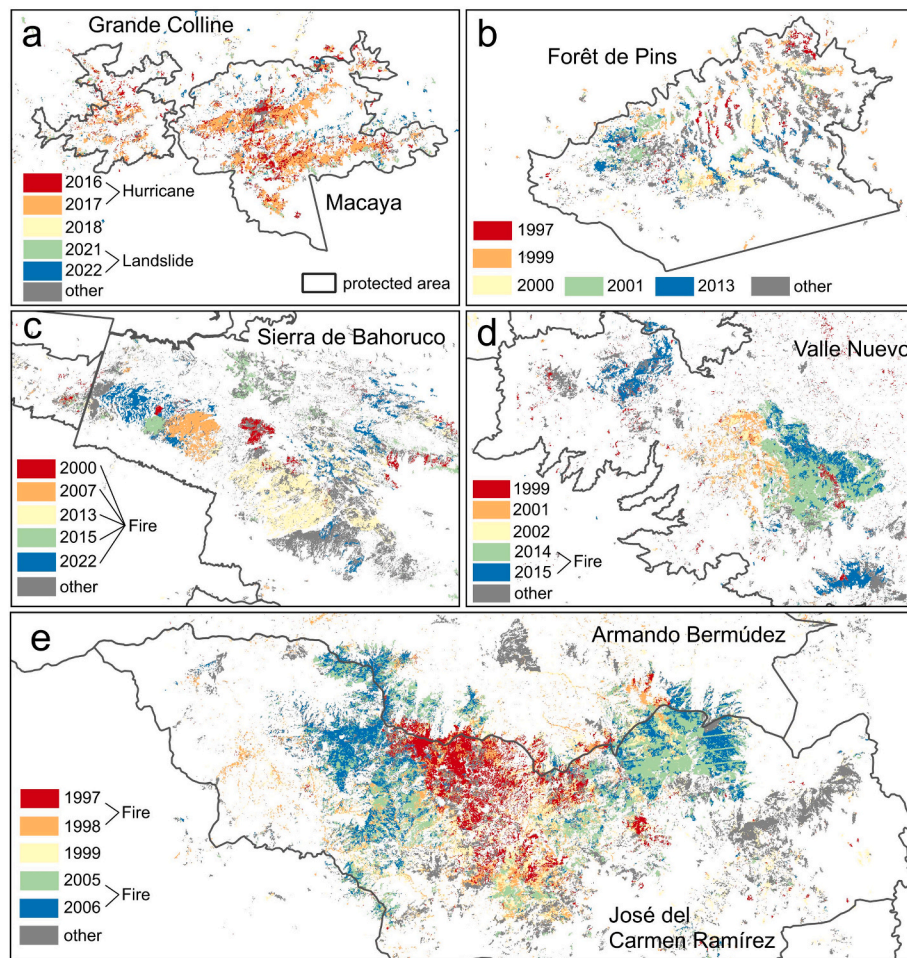


Fig. 8. Five examples of hotspots of primary forest (PF) loss in Hispaniola. Subplots (a) through (e) correspond to the hotspots A through E in Fig. 5c, respectively. The black boundary denotes the protected area boundary with the name annotated. The numbers indicate the top five years with the most significant PF loss. The major events/drivers causing the PF loss in specific years were provided. PF loss in the remaining years is categorized as “other” and is displayed using gray pixels.

strong disturbance. Strong disturbances, such as tree-cutting, can permanently alter the PF structure and significantly reduce the NBR index (Fig. 4b). However, the impact of disturbances on PF structure and the NBR index can also depend on the resilience of PF. Weak disturbance can significantly reduce the NBR index in PF with low resilience. Fragmentation of PF can reduce its resilience and intensify the impact of disturbances on forest structure and the corresponding spectral response (Hansen et al., 2020). There are various ways to consider forest resilience, and the definition of resilience varies among studies (Poorter et al., 2016). In our study, spectral change measured by Landsat time series offers an effective way to consider resilience in large-scale PF mapping (White et al., 2017). Combining this with other contextual information, such as the field measurement reports, can improve resilience measurement (Kennedy et al., 2012).

Our study applied the dense Landsat time series to continuously map PF and SF in Hispaniola. We conducted a comprehensive evaluation of PF disparity between Haiti and the Dominican Republic, a comparison not previously undertaken by other studies. We compared the PF conversion pattern, PF status inside and outside protected areas, and PF fragmentation levels (Fig. 7, Fig. 10 & Fig. 13). Our comparison results demonstrate that there is less PF in Haiti and it is more fragmented than in the Dominican Republic, indicating a need for more urgent conservation action for PF in Haiti. Our analysis also highlights widespread PF loss inside and outside protected areas of Hispaniola. To accurately assess the effectiveness of protection policy on PF, it is important to consider PF outside of the protected areas with similar spatial and

climatic characteristics (Geldmann et al., 2019; Liang et al., 2023). However, the widespread PF loss within protected areas revealed in our study raises concerns for policymakers who need to improve protection strategies (John and Yolanda, 2019; Sangermano et al., 2015b).

Additionally, we found SFs are increasing in the two countries due to the conversion of PF and forest regrowth, resulting in an overall increase in total forest area. This resolves the contradictory findings from previous studies on whether the tree cover is increasing or decreasing in Haiti and the Dominican Republic, which often conflated PF and SF (Churches et al., 2014; John and Yolanda, 2019; Pauleus and Aide, 2020; Rodrigues-Eklund et al., 2021; Sangermano et al., 2015a). Our map results supported previous work (e.g., Hedges et al. (2018)) showing that PF often occupies a small portion of the FAO-defined “forest”, which is “land spanning more than 0.5 hectares with trees higher than 5 meters and a canopy cover of more than 10 percent, or trees able to reach these thresholds in situ” (FAO, 2015). Conflating PF and SF could have disastrous consequences for biodiversity conservation. More analysis and mapping of PF are needed globally to mitigate this problem.

The land cover maps also show that more than half of the land surface in Haiti is covered with barren, cropland (active and abandoned), or other deforested surface. This is surprising because various types of vegetation (e.g., SF) can grow on poor soil, so why isn't it vegetated? This is likely because of intensive and successive agricultural activities in the 20th century (Hedges et al., 2018; Marzelius and Droste, 2022). The large charcoal market, which provides energy for cooking, probably

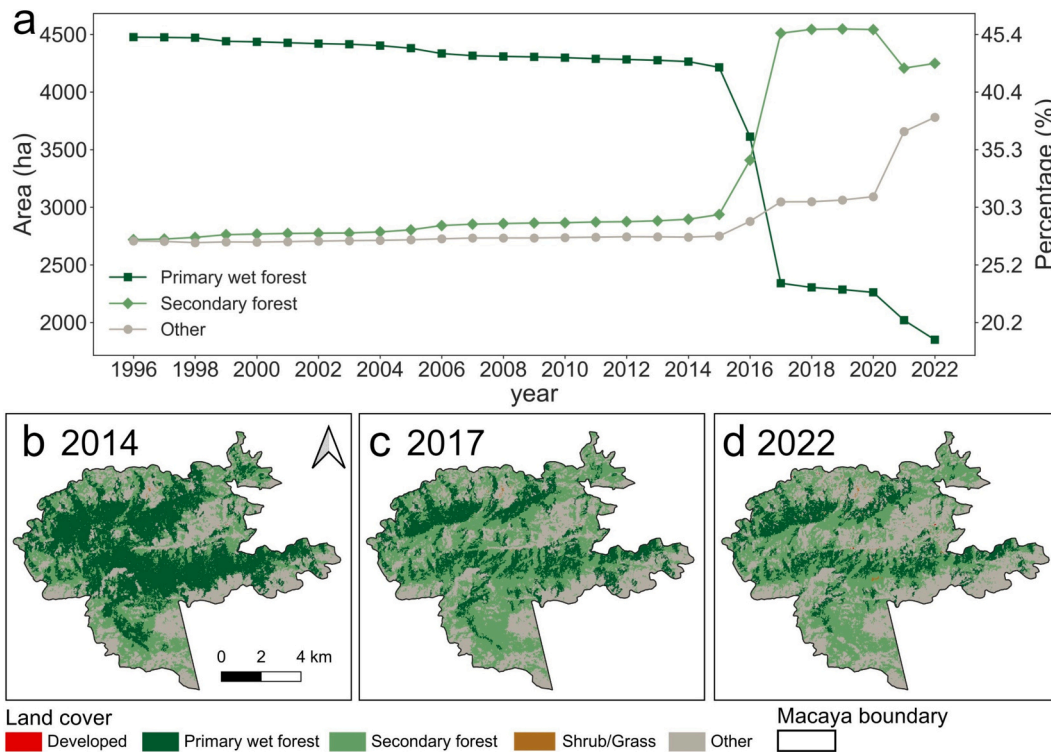


Fig. 9. Impacts of 2016 Hurricane Matthew and the 2021 Haiti earthquake on the land cover change in Macaya National Park (located in Hotspot A, Fig. 5c). (a) Map-based area (left y-axes) and percentage (right y-axes) of primary wet forest, secondary forest and other types in Macaya National Park from 1996 to 2022. (b)–(d) Land cover maps of Macaya National Park in 2014, 2017, and 2022, respectively.

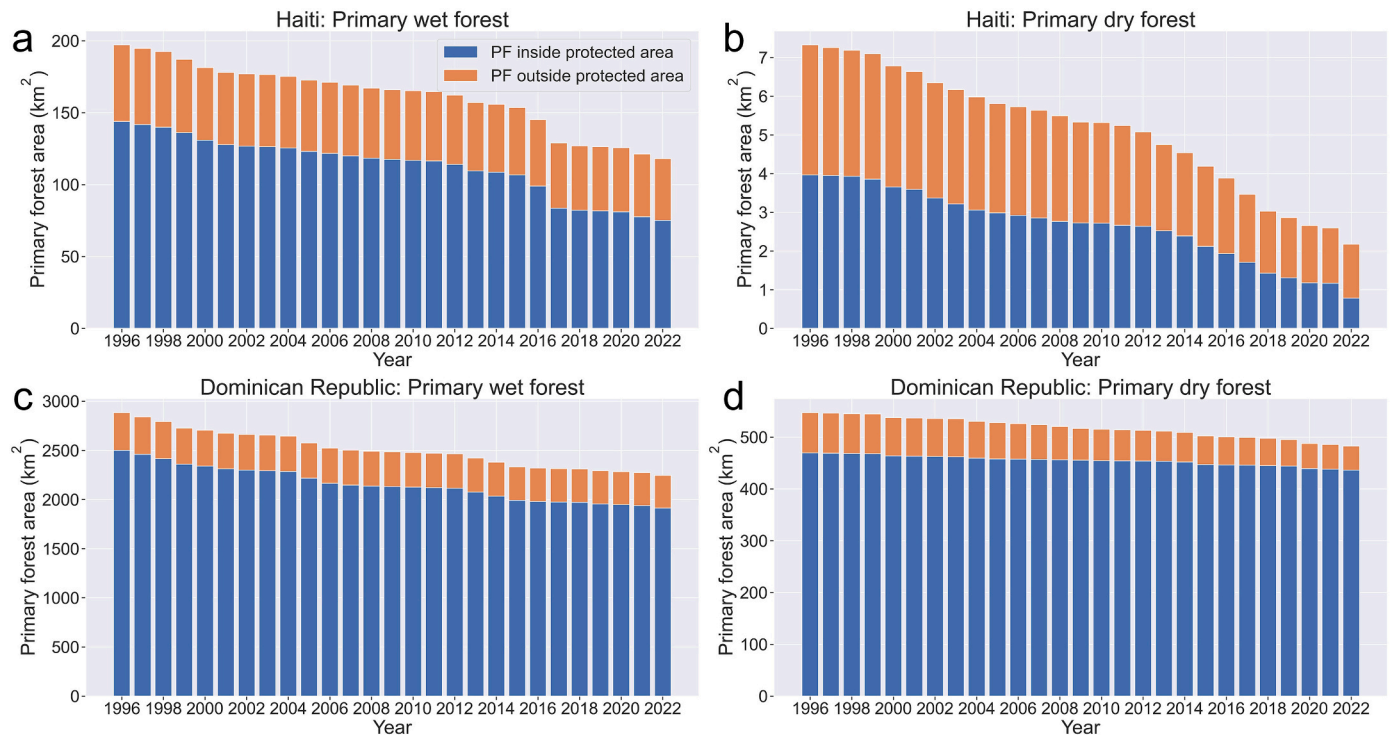


Fig. 10. Map-based primary forests (including primary wet and dry forests) area variation inside and outside protected areas. (a) Primary wet forest change in Haiti; (b) Primary dry forest change in Haiti; (c) Primary wet forest change in the Dominican Republic; (d) Primary dry forest change in the Dominican Republic.

explains some of this. Charcoal can be made from small stems (seedlings) and therefore plants never have a chance of growing. Additionally, continued deforestation over many decades (or centuries) can cause

desertification and severe erosion, whereby the land can no longer support vegetation (Cohen, 1984).

Furthermore, we quantified the drivers of PF loss in Hispaniola and

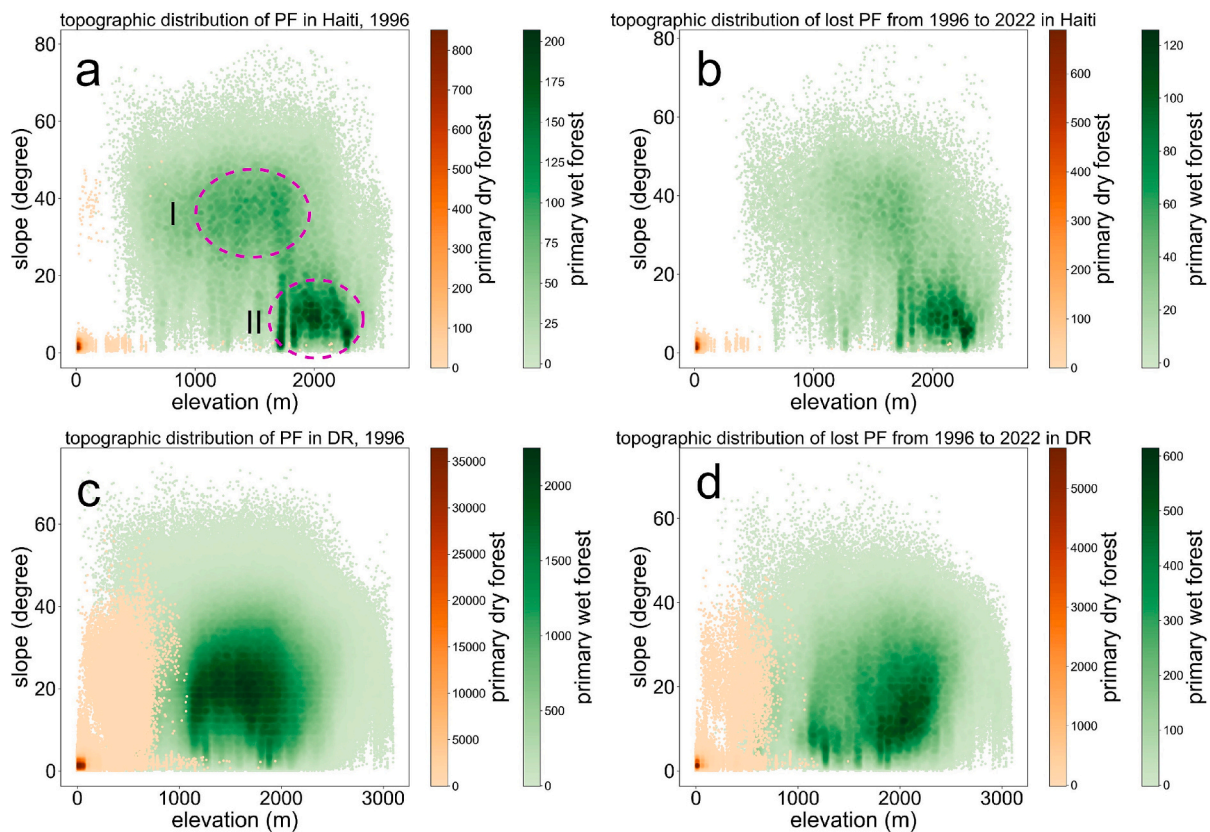


Fig. 11. Topographic characteristics of primary wet and dry forest distribution and loss. Subplot (a) shows the topographic distribution of primary forests (PFs) in Haiti as of 1996. Subplot (b) shows the topographic distribution of lost PF in Haiti between 1996 and 2022. Subplots (c) and (d) correspond to subplots (a) and (b), respectively, for the Dominican Republic (DR). The orange and green colour bars represent the primary dry and wet forests, respectively. The values indicate point density, where larger values and darker colors correspond to higher point density. (For interpretation of the references to colour in this figure legend, the reader is referred to the web version of this article.)

identified the PF loss hotspots. The analysis of PF loss hotspots indicates that extreme events such as fires, hurricanes, and landslides caused by earthquakes significantly contribute to PF loss in Hispaniola (Fig. 8). The impacts of extreme events can be compounded by anthropogenic activities. These large-scale fires (Fig. 8), most of which are likely human-sparked wildfires that happened in pine-dominated PF (S.B.H. and J.T. personal observations), are much more destructive than those caused by nature (Balch et al., 2017; Hantson et al., 2022). With increased human activities encroaching into remote primary forests, PF loss caused by human-induced fires is expected to intensify in the future. The forest fragmentation caused by human activities likely has accelerated PF loss during hurricanes and landslides. Extensive fragmentation of forests on the island exposes otherwise protected forests to wind damage and biomass loss (Laurance et al., 1997), preconditioning the forests to damage from hurricanes. In turn, deforestation reduces soil integrity created by roots, thus preconditioning the forests for further loss from landslides during earthquakes (Havenith et al., 2022). While earthquakes are natural events, hurricanes are believed to be strengthening due to human-caused climate change (Knutson et al., 2010). The findings underscore the urgent need for effective conservation policies and interventions to mitigate the impacts of both anthropogenic and natural disturbances on PFs in Hispaniola.

5.2. Uneven Landsat image density in Hispaniola

Landsat density, i.e., the frequency of clear Landsat observations, can affect the fitting of the COLD algorithm and change detection (Tollerud et al., 2023; Zhang et al., 2021). Hispaniola has fewer clear observations compared to data-rich regions, such as the United States (Zhang et al.,

2022). The Landsat data for Hispaniola is unevenly distributed in space and time (Fig. 14), which brings uncertainties in land cover mapping and disturbance detection. The eastern Dominican Republic has fewer clear Landsat observations than other regions in Hispaniola due to frequent cloud cover. This might lead to the underestimation of disturbance in those regions. Fortunately, the eastern Dominican Republic covers only a small proportion of primary dry forest, which has limited impacts on PF loss monitoring.

The temporal density of Landsat observations is influenced by the number of operational Landsat satellites. Before 2000, Landsat 5 was the dominant satellite in operation, but a single satellite can only provide limited clear observations. When Landsat 7 became operational after 2000, the average of clear observations per year increased slightly from 5.8 images/year to 7.3 images/year (Fig. 14). This was due to the Landsat 7 Scan Line Corrector (SLC) failure and the limited capacity of USGS to store those historical Landsat images. Fortunately, the situation improved significantly with the launch of Landsat 8 in 2013. Furthermore, the release of Landsat 9 data in October 2021 ensures sufficient clear observations for monitoring disturbance (Fig. 14d).

To cope with the uneven distribution of limited Landsat clear observations and capture all potential land disturbances, especially for PFs, which are sensitive to subtle disturbances, we employed a sensitive parameter setting for COLD (Zhu et al., 2020). This might cause some commission errors in the primary wet forest disturbance detection, but the NBR threshold can greatly reduce the negative impact of commission error (Fig. 3). More commission errors might also be created for other land disturbances. However, the land cover classification might still be the same as the pre-disturbance classification, which can eliminate the impact of more commission errors in land change detection.

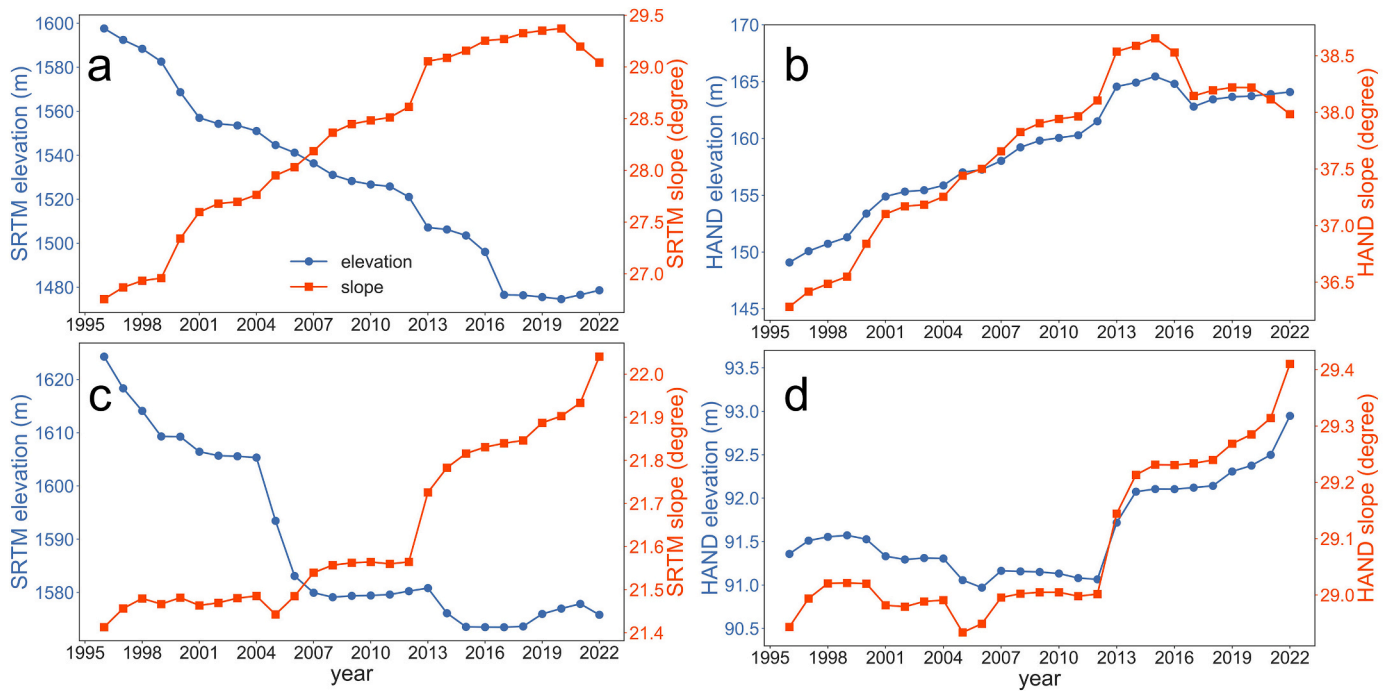


Fig. 12. Mean elevation (blue lines) and slope (orange lines) change of primary wet forest from 1996 to 2022. Subplots (a) and (b) display the results with SRTM (Shuttle Radar Topography Mission) and HAND (Height Above the Nearest Drainage) elevation datasets in Haiti, respectively. Subplots (c) and (d) are the same as (a) and (b), but for the Dominican Republic, respectively. (For interpretation of the references to colour in this figure legend, the reader is referred to the web version of this article.)

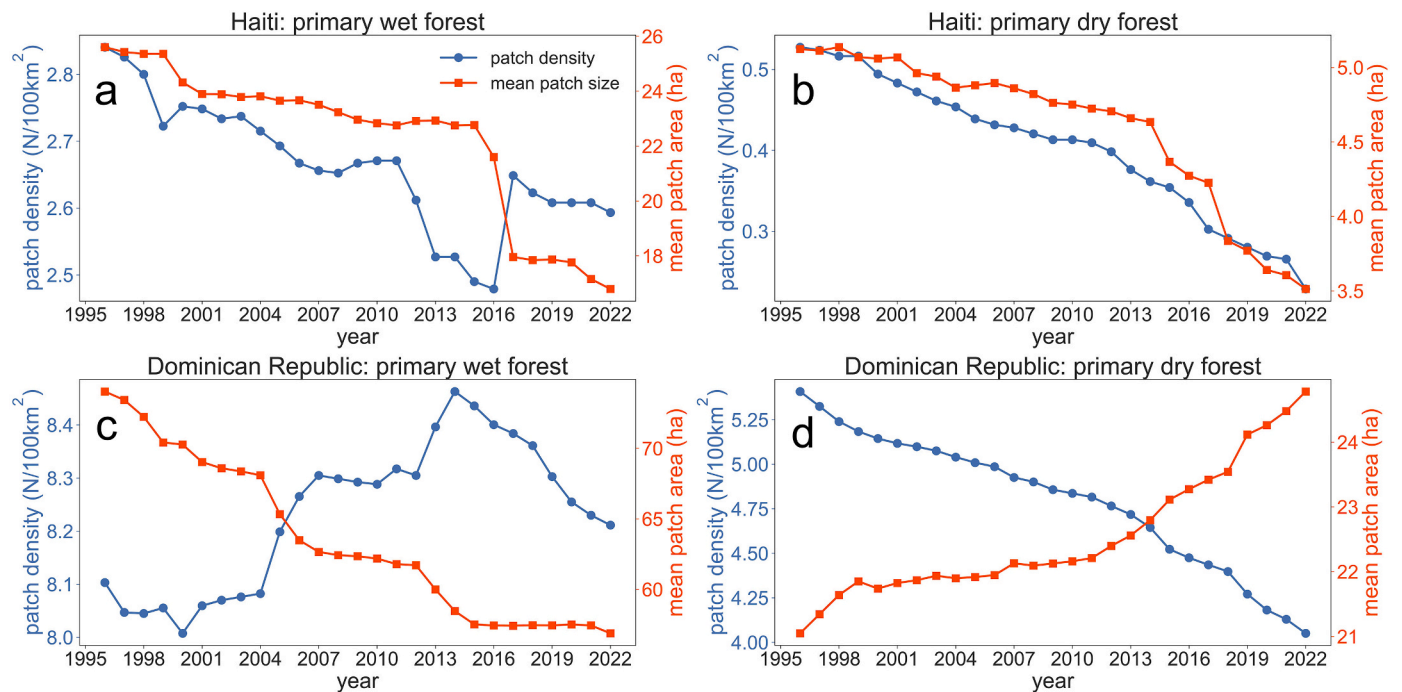


Fig. 13. Fragmentation level analysis for primary forest in Hispaniola. Subplot (a) shows the patch density (patch numbers per 100 km²) and mean patch area of the primary wet forest in Haiti. Subplots (b), (c) and (d) are the same as subplot (a), but for primary dry forest in Haiti, primary wet forest in the Dominican Republic, and primary dry forest in the Dominican Republic, respectively. The blue curves and left y-axis denote the patch density. The orange curves and right y-axis denote the mean patch area. (For interpretation of the references to colour in this figure legend, the reader is referred to the web version of this article.)

6. Conclusion

Distinguishing PF and SF using remote sensing observations is critical for evaluating the impact of forest loss on biodiversity, which is

rarely done in tropical regions. Our study used dense Landsat time series and the COLD algorithm to map annual PF changes in Haiti and the Dominican Republic from 1996 to 2022. We successfully distinguished PF and SF with an overall accuracy of 80.5% ($\pm 5.2\%$) for the land cover

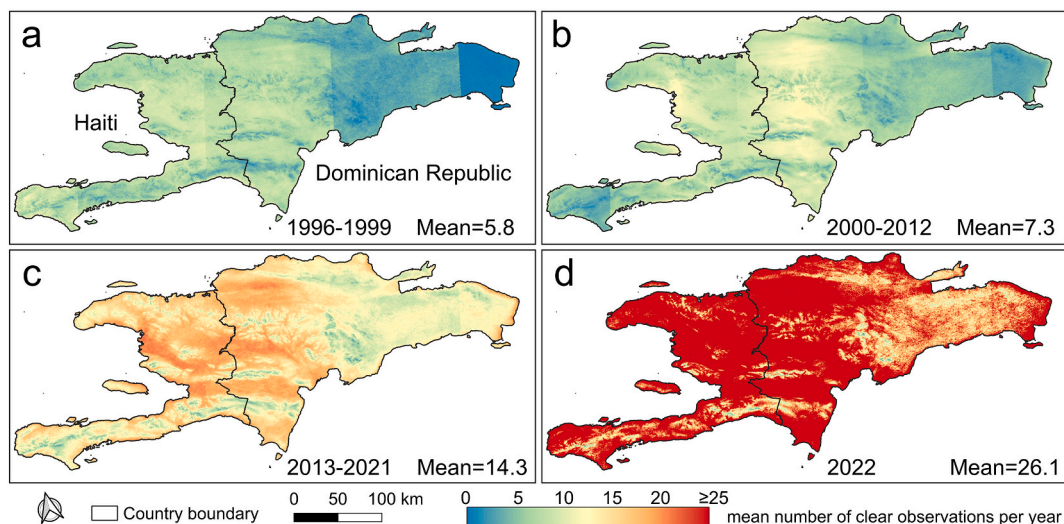


Fig. 14. The mean number of clear observations per year used as input for time series analysis in Hispaniola. (a) from 1996 to 1999 with Landsat 4 and 5 mainly in operation. (b) from 2000 to 2012 with Landsat 5 and 7 mainly in operation. (c) from 2013 to 2021 with Landsat 7 and 8 mainly in operation. (d) In 2022 with Landsat 8 and 9 mainly in operation. The numbers in the lower right corner represent the mean value for all of Hispaniola.

classification. The major conclusions include: (1) From 1996 to 2022, both Haiti and the Dominican Republic experienced rapid PF loss, inside and outside protected areas, indicating that those areas are ineffective. Map-based results indicate that Haiti’s PF decreased from 0.75% to 0.44% and the Dominican Republic’s PF decreased from 7.14% to 5.67%. Haiti has a higher proportion of PF directly converted to non-forest surface. (2) Haiti exhibits significantly greater PF fragmentation compared to the Dominican Republic. This higher degree of fragmentation further threatens Haiti’s remaining PF and its associated biodiversity. (3) Slope plays a crucial role in the PF loss. PF in regions with steeper slopes tends to be less accessible to humans, thus experiencing less PF loss. (4) The major driver of PF loss in Hispaniola is fire. This is followed by tree-cutting, hurricanes, and landslides. The generated land cover map can be valuable in guiding the PF and biodiversity conservation efforts. With training data collected from other locations, this approach could be applied to other regions and at larger scales.

CRedit authorship contribution statement

Falu Hong: Writing – original draft, Validation, Software, Methodology, Investigation, Formal analysis, Data curation, Conceptualization.

S. Blair Hedges: Writing – review & editing, Supervision, Resources, Project administration, Methodology, Funding acquisition, Data curation, Conceptualization. **Zhiqiang Yang:** Writing – review & editing, Supervision, Conceptualization. **Ji Won Suh:** Writing – review & editing, Validation. **Shi Qiu:** Writing – review & editing, Validation. **Joel Timyan:** Writing – review & editing, Data curation. **Zhe Zhu:** Writing – review & editing, Validation, Supervision, Resources, Project administration, Methodology, Funding acquisition, Data curation, Conceptualization.

Declaration of competing interest

The authors declare that they have no known competing financial interests or personal relationships that could have appeared to influence the work reported in this paper.

Acknowledgment

This work was supported by a grant from the NSF Biodiversity on a Changing Planet (BoCP) program (2326013 to S.B.H. and 2326014 to Z. Z.).

Appendix A. Statistical results and examples of collected training sample

Table A1
Statistical results of collected training sample.

Land cover	Count of digitized polygons	Count of pixels	Count of selected training sample
Developed	59	26,620	1,206
Primary wet forest	46	25,476	1,341
Primary dry forest	6	47,221	752
Secondary forest	63	11,606	7,973
Shrub / Grass	106	41,890	1,823
Water	34	70,518	768
Wetland	38	10,171	771
Other	198	108,511	10,449
Sum	550	342,013	25,083

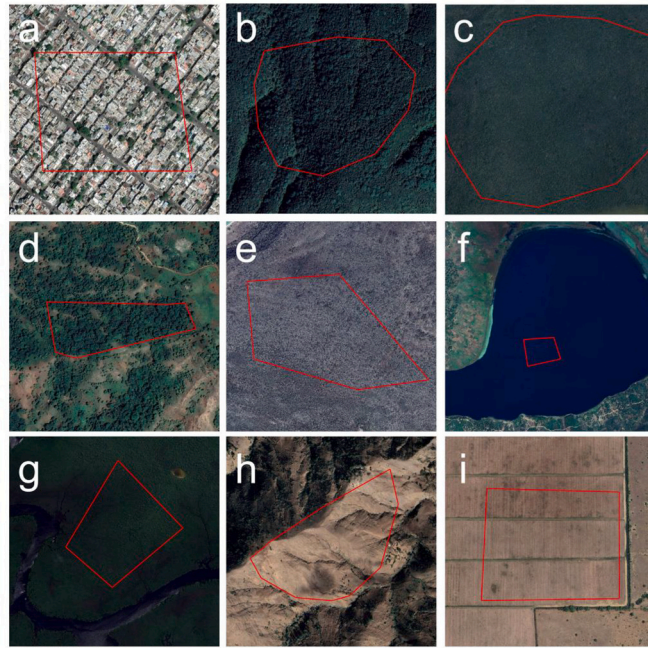


Fig. A1. Examples showing high-resolution images of training sample. (a) Developed; (b) Primary wet forest; (c) Primary dry forest; (d) Secondary forest; (e) Shrub/Grass; (f) Water; (g) Wetland; (h) Other-barren; (i) Other-cropland.

Appendix B. Vegetation index changes for different disturbance agents

We selected five vegetation indices to compare their capability of distinguishing between the recovered PF and SF: Normalized Difference Vegetation Index (NDVI) (Tucker, 1979), kNDVI (Camps-Valls et al., 2021), Normalized Burn Ratio (NBR) (Key and Benson, 2006), Enhanced Vegetation Index (EVI) (Huete et al., 2002), and Normalized Difference Fraction Index (NDFI) (Bullock et al., 2020; Souza et al., 2005).

The equations to calculate the selected vegetation indices are given as follows.

(1) Normalized Difference Vegetation Index (NDVI) (Tucker, 1979)

$$NDVI = \frac{NIR - Red}{NIR + Red} \quad (2)$$

where NIR and Red represent the surface reflectance of near infrared and red bands of Landsat.

(2) kNDVI (Camps-Valls et al., 2021)

We used the simplified version of kNDVI index as displayed in Eq. (3).

$$kNDVI = \tanh(NDVI^2) \quad (3)$$

(3) Normalized Burn Ratio (NBR) (Key and Benson, 2006)

$$NBR = \frac{NIR - SWIR2}{NIR + SWIR2} \quad (4)$$

where SWIR2 represents the surface reflectance of Shortwave Infrared (SWIR) 2 band of Landsat.

(4) EVI (Huete et al., 2002)

$$EVI = 2.5 * \frac{NIR - Red}{NIR + 6 * Red - 7.5 * Blue + 1} \quad (5)$$

where Blue represents surface reflectance of blue band of Landsat.

(5) Normalized Difference Fraction Index (NDFI) (Bullock et al., 2020; Souza et al., 2005)

$$NDFI = \frac{GV_{shade} - (NPV + Soil)}{GV_{shade} + (NPV + Soil)} \tag{6}$$

where GV_{shade} is calculated as:

$$GV_{shade} = \frac{GV}{1 - Shade} \tag{7}$$

The green vegetation (GV), non-photosynthetic vegetation (NPV), Soil, Shade parameters represent the fraction of endmembers. The endmembers are calculated as the linear combination of different Landsat bands. The coefficients are provided in Bullock et al. (2020). The fraction of the endmembers is calculated by spectral unmixing following the simple linear mixture model.

The boxplots show the VI changes before and after different disturbance agents (Fig. 3 & Fig. B1). The results show that VI changes caused by fire, hurricanes, landslides, and tree-cutting are more significant compared to those caused by drought. Compared with NBR, it is challenging for NDVI, kNDVI, EVI, and NDFI to find a single threshold to separate the strong disturbances and weak disturbances. Therefore, we used NBR and the threshold of 0.05 in the PF post-processing.

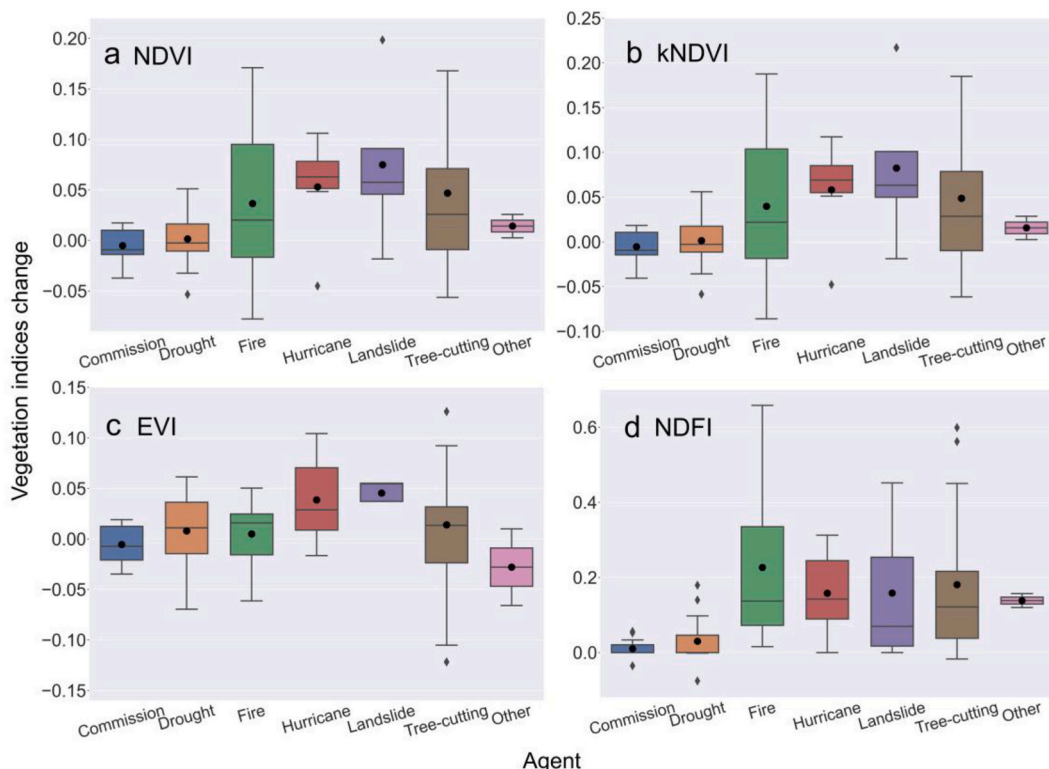


Fig. B1. Boxplots showing changes in vegetation indices (VIs) for different disturbance agents, which are calculated by subtracting post-disturbance VIs from pre-disturbance VIs. (a) Normalized Difference Vegetation Index (NDVI); (b) kNDVI; (c) Enhanced Vegetation Index (EVI); (d) Normalized Difference Fraction Index (NDFI). The meanings of each component in the boxplot are the same as those in Fig. 3.

Appendix C. Sample-based confusion matrices of land cover classification and primary forest loss detection

Table C1

Confusion matrix of land cover classification in sample counts. PWF, PDF, and SF indicate primary wet forest, primary dry forest, and secondary forest, respectively.

Map	Reference									Weight (%)
	Developed	PWF	PDF	SF	Shrub/Grass	Water	Wetland	Other	Total	
Developed	17	0	0	1	0	0	0	3	21	1.44
PWF	0	41	0	8	0	0	0	0	49	3.55
PDF	0	1	43	6	0	0	0	0	50	0.70
SF	0	1	0	57	3	0	0	12	73	39.09
Shrub/Grass	0	0	0	10	9	0	0	4	23	2.39
Water	0	0	0	0	0	23	1	1	25	0.91
Wetland	0	0	1	3	0	4	16	0	24	0.60
Other	0	0	0	12	3	0	2	89	106	51.33
Total	17	43	44	97	15	27	19	109	371	

Table C2
Confusion matrix of primary forest (PF) loss detection in sample counts.

Map	Reference			Weight (%)
	Other	PF loss	Total	
Other	383	1	384	98.95
PF loss	30	66	96	1.05
Total	413	67	480	

Data availability

The generated land cover map is freely available at <https://doi.org/10.6084/m9.figshare.28100408> and Google Earth Engine (<https://gers.users.earthengine.app/view/hispaniola-1c>). The corresponding code is available at https://github.com/faluhong/hispaniola_land_cover_mapping.

References

- Aide, T.M., Clark, M.L., Grau, H.R., López-Carr, D., Levy, M.A., Redo, D., Bonilla-Moheno, M., Riner, G., Andrade-Núñez, M.J., Muñiz, M., 2013. Deforestation and reforestation of Latin America and the Caribbean (2001–2010). *Biotropica* 45, 262–271.
- Aloy, J., 2017. Effects of habitat disturbance on tropical forest biodiversity. *Proc. Natl. Acad. Sci.* 114, 6056–6061.
- Álvarez-Berrios, N., Redo, D., Aide, T., Clark, M., Grau, R., 2013. Land change in the Greater Antilles between 2001 and 2010. *Land* 2, 81–107.
- Arévalo, P., Olofsson, P., Woodcock, C.E., 2020. Continuous monitoring of land change activities and post-disturbance dynamics from Landsat time series: A test methodology for REDD+ reporting. *Remote Sens. Environ.* 238, 111051.
- Balch, J.K., Bradley, B.A., Abatzoglou, J.T., Nagy, R.C., Fusco, E.J., Mahood, A.L., 2017. Human-started wildfires expand the fire niche across the United States. *Proc. Natl. Acad. Sci.* 114, 2946–2951.
- Barlow, J., Gardner, T.A., Araujo, I.S., Ávila-Pires, T.C., Bonaldo, A.B., Costa, J.E., Esposito, M.C., Ferreira, L.V., Hawes, J., Hernandez, M.I.M., Hoogmoed, M.S., Leite, R.N., Lo-Man-Hung, N.F., Malcolm, J.R., Martins, M.B., Mestre, L.A.M., Miranda-Santos, R., Nunes-Gutjahr, A.L., Overal, W.L., Parry, L., Peters, S.L., Ribeiro-Junior, M.A., da Silva, M.N.F., da Silva Motta, C., Peres, C.A., 2007. Quantifying the biodiversity value of tropical primary, secondary, and plantation forests. *Proc. Natl. Acad. Sci.* 104, 18555–18560.
- Belgiu, M., Drăguț, L., 2016. Random forest in remote sensing: A review of applications and future directions. *ISPRS J. Photogramm. Remote Sens.* 114, 24–31.
- Bernier, P.Y., Paré, D., Stinson, G., Bridge, S.R.J., Kishchuk, B.E., Lemprière, T.C., Thiffault, E., Titus, B.D., Vasbinder, W., 2017. Moving beyond the concept of “primary forest” as a metric of forest environment quality. *Ecol. Appl.* 27, 349–354.
- Brooks, T.M., Mittermeier, R.A., Mittermeier, C.G., Da Fonseca, G.A.B., Rylands, A.B., Konstant, W.R., Flick, P., Pilgrim, J., Oldfield, S., Magin, G., Hilton-Taylor, C., 2002. Habitat loss and extinction in the hotspots of biodiversity. *Conserv. Biol.* 16, 909–923.
- Brown, J.F., Tollerud, H.J., Barber, C.P., Zhou, Q., Dwyer, J.L., Vogelmann, J.E., Loveland, T.R., Woodcock, C.E., Stehman, S.V., Zhu, Z., Pengra, B.W., Smith, K., Horton, J.A., Xian, G., Auch, R.F., Sohl, T.L., Saylor, K.L., Gallant, A.L., Zelenak, D., Reker, R.R., Rover, J., 2020. Lessons learned implementing an operational continuous United States national land change monitoring capability: The Land Change Monitoring, Assessment, and Projection (LCMAP) approach. *Remote Sens. Environ.* 238, 111356.
- Bullock, E.L., Woodcock, C.E., Olofsson, P., 2020. Monitoring tropical forest degradation using spectral unmixing and Landsat time series analysis. *Remote Sens. Environ.* 238.
- Camps-Valls, G., Campos-Taberner, M., Moreno-Martínez, Á., Walther, S., Duveiller, G., Cescatti, A., Mahecha, M.D., Muñoz-Marí, J., García-Haro, F.J., Guanter, L., Jung, M., Gamon, J.A., Reichstein, M., Running, S.W., 2021. A unified vegetation index for quantifying the terrestrial biosphere. *Sci. Adv.* 7, eabc7447.
- Churches, C.E., Wampler, P.J., Sun, W., Smith, A.J., 2014. Evaluation of forest cover estimates for Haiti using supervised classification of Landsat data. *Int. J. Appl. Earth Obs. Geoinf.* 30, 203–216.
- Cohen, W.B., 1984. Environmental degradation in Haiti: an analysis of aerial photography. US Agency for International Development/Haiti, Port-au-Prince, Haiti.
- Cohen, W.B., Yang, Z., Healey, S.P., Kennedy, R.E., Gorelick, N., 2018. A LandTrendr multispectral ensemble for forest disturbance detection. *Remote Sens. Environ.* 205, 131–140.
- De Giorgi, A., Solarna, D., Moser, G., Tapete, D., Cigna, F., Boni, G., Rudari, R., Serpico, S.B., Pisani, A.R., Montuori, A., Zoffoli, S., 2021. Monitoring the recovery after 2016 Hurricane Matthew in Haiti via markovian multitemporal region-based modeling. *Remote Sens.* 13, 3509.
- Decuyper, M., Chávez, R.O., Lohbeck, M., Lastra, J.A., Tsendbazar, N., Hackländer, J., Herold, M., Vágen, T.-G., 2022. Continuous monitoring of forest change dynamics with satellite time series. *Remote Sens. Environ.* 269, 112829.
- Donchyts, G., Winsemius, H., Schellekens, J., Erickson, T., Gao, H., Savenije, H., van de Giesen, N., 2016. Global 30m height above the nearest drainage. HAND 1000.
- FAO, 2015. Global Forest Resources Assessments 2015: Terms and Definitions. In: FAO Report.
- Fernández, E., 2007. Hispaniola: A Photographic Journey Through Island Biodiversity, Biodiversidad a Través de Un Recorrido Fotográfico. Harvard University Press/Belknap Press, Cambridge, MA.
- Friedl, M.A., Woodcock, C.E., Olofsson, P., Zhu, Z., Loveland, T., Stanimirova, R., Arevalo, P., Bullock, E., Hu, K.-T., Zhang, Y., Turlej, K., Tarrio, K., McAvoy, K., Gorelick, N., Wang, J.A., Barber, C.P., Souza, C., 2022. Medium spatial resolution mapping of global land cover and land cover change across multiple decades from Landsat. *Front. Remote Sens.* 3.
- Geldmann, J., Manica, A., Burgess, N.D., Coad, L., Balmford, A., 2019. A global-level assessment of the effectiveness of protected areas at resisting anthropogenic pressures. *Proceedings of the National Academy of Sciences* 116, 23209–23215.
- Gibson, L., Lee, T.M., Koh, L.P., Brook, B.W., Gardner, T.A., Barlow, J., Peres, C.A., Bradshaw, C.J.A., Laurance, W.F., Lovejoy, T.E., Sodhi, N.S., 2011. Primary forests are irreplaceable for sustaining tropical biodiversity. *Nature* 478, 378–381.
- Hansen, M.C., Potapov, P.V., Moore, R., Hancher, M., Turubanova, S.A., Tyukavina, A., Thau, D., Stehman, S.V., Goetz, S.J., Loveland, T.R., Kommareddy, A., Egorov, A., Chini, L., Justice, C.O., Townshend, J.R.G., 2013. High-resolution global maps of 21st-century forest cover change. *Science* 342, 850–853.
- Hansen, M.C., Wang, L., Song, X.-P., Tyukavina, A., Turubanova, S., Potapov, P.V., Stehman, S.V., 2020. The fate of tropical forest fragments. *Sci. Adv.* 6, eaax8574.
- Hanson, S., Andela, N., Goulden, M.L., Randerson, J.T., 2022. Human-ignited fires result in more extreme fire behavior and ecosystem impacts. *Nat. Commun.* 13, 2717.
- Havenith, H.B., Guerrier, K., Schlögel, R., Braun, A., Ulysse, S., Mreyen, A.S., Victor, K. H., Saint-Fleur, N., Cauchie, L., Boisson, D., Prépétit, C., 2022. Earthquake-induced landslides in Haiti: analysis of seismotectonic and possible climatic influences. *Nat. Hazards Earth Syst. Sci.* 22, 3361–3384.
- Hedges, S.B., Cohen, W.B., Timyan, J., Yang, Z., 2018. Haiti’s biodiversity threatened by nearly complete loss of primary forest. *Proc. Natl. Acad. Sci.* 115, 11850–11855.
- Heinrich, V.H.A., Vancutsem, C., Dalagnol, R., Rosan, T.M., Fawcett, D., Silva-Junior, C. H.L., Cassol, H.L.G., Achard, F., Jucker, T., Silva, C.A., House, J., Sitch, S., Hales, T. C., Aragão, L.E.O.C., 2023. The carbon sink of secondary and degraded humid tropical forests. *Nature* 615, 436–442.
- Huete, A., Didan, K., Miura, T., Rodriguez, E.P., Gao, X., Ferreira, L.G., 2002. Overview of the radiometric and biophysical performance of the MODIS vegetation indices. *Remote Sens. Environ.* 83, 195–213.
- ITTO, 2002. ITTO guidelines for the restoration, management and rehabilitation of degraded and secondary tropical forests. International Tropical Timber Organization.
- John, D.L., Yolanda, M.L., 2019. Forest change within and outside protected areas in the Dominican Republic, 2000–2016. *bioRxiv*, 558346.
- Kennedy, R.E., Yang, Z., Cohen, W.B., Pfaff, E., Braaten, J., Nelson, P., 2012. Spatial and temporal patterns of forest disturbance and regrowth within the area of the Northwest Forest Plan. *Remote Sens. Environ.* 122, 117–133.
- Key, C., Benson, N., 2006. Landscape assessment: remote sensing of severity, the normalized burn ratio and ground measure of severity, the composite burn index. *FIREMON: Fire effects monitoring and inventory system Ogden*. USDA Forest Service, Rocky Mountain Res. Station, Utah.
- Knorn, J.A.N., Kuemmerle, T., Radeloff, V.C., Keeton, W.S., Gancz, V., Biriş, I.-A., Svoboda, M., Griffiths, P., Hagatis, A., Hostert, P., 2013. Continued loss of temperate old-growth forests in the Romanian Carpathians despite an increasing protected area network. *Environ. Conserv.* 40, 182–193.
- Knutson, T.R., McBride, J.L., Chan, J., Emanuel, K., Holland, G., Landsea, C., Held, I., Kossin, J.P., Srivastava, A.K., Sugi, M., 2010. Tropical cyclones and climate change. *Nat. Geosci.* 3, 157–163.
- Kormos, C.F., Mackey, B., DellaSala, D.A., Kumpe, N., Jaeger, T., Mittermeier, R.A., Filardi, C., 2018. Primary forests: Definition, status and future prospects for global conservation. *Encyclopedia. Anthropol.* 31–41.
- Laurance, W.F., Laurance, S.G., Ferreira, L.V., Rankin-de Merona, J.M., Gascon, C., Lovejoy, T.E., 1997. Biomass collapse in Amazonian forest fragments. *Science* 278, 1117–1118.
- Liang, M., González-Roglich, M., Roehrdanz, P., Tabor, K., Zvoleff, A., Leitold, V., Silva, J., Fatoyinbo, T., Hansen, M., Duncanson, L., 2023. Assessing protected area’s carbon stocks and ecological structure at regional-scale using GEDI lidar. *Global Environmental Change* 78, 102621.

- Martin, P.H., Sherman, R.E., Fahey, T.J., 2004. Forty years of tropical forest recovery from agriculture: Structure and floristics of secondary and old-growth riparian forests in the Dominican Republic. *Biotropica* 36, 297–317.
- Marzelius, M., Droste, N., 2022. Livelihoods matter – A comparative political ecology of forest use on Hispaniola. *Forest Policy Econ.* 141, 102765.
- Mikoláš, M., Ujházy, K., Jasík, M., Wizek, M., Gally, L., Polák, P., Vysoký, J., Čiliák, M., Meigs, G.W., Svoboda, M., Trotsiuk, V., Keeton, W.S., 2019. Primary forest distribution and representation in a Central European landscape: Results of a large-scale field-based census. *For. Ecol. Manag.* 449, 117466.
- Mikoláš, M., Piovesan, G., Ahlström, A., Donato, D.C., Gloor, R., Hofmeister, J., Keeton, W.S., Muys, B., Sabatini, F.M., Svoboda, M., Kuemmerle, T., 2023. Protect old-growth forests in Europe now. *Science* 380, 466.
- Myers, N., Mittermeier, R.A., Mittermeier, C.G., da Fonseca, G.A.B., Kent, J., 2000. Biodiversity hotspots for conservation priorities. *Nature* 403, 853–858.
- Nobre, A.D., Cuartas, L.A., Hodnett, M., Rennó, C.D., Rodrigues, G., Silveira, A., Waterloo, M., Saleska, S., 2011. Height Above the Nearest Drainage – a hydrologically relevant new terrain model. *J. Hydrol.* 404, 13–29.
- Olofsson, P., Foody, G.M., Herold, M., Stehman, S.V., Woodcock, C.E., Wulder, M.A., 2014. Good practices for estimating area and assessing accuracy of land change. *Remote Sens. Environ.* 148, 42–57.
- Olofsson, P., Arévalo, P., Espejo, A.B., Green, C., Lindquist, E., McRoberts, R.E., Sanz, M. J., 2020. Mitigating the effects of omission errors on area and area change estimates. *Remote Sens. Environ.* 236, 111492.
- Palahí, M., Valbuena, R., Senf, C., Acil, N., Pugh, T.A.M., Sadler, J., Seidl, R., Potapov, P., Gardiner, B., Hetemäki, L., Chirici, G., Francini, S., Hlásny, T., Lerink, B.J.W., Olsson, H., González Olabarria, J.R., Ascoli, D., Asikainen, A., Bauhus, J., Berndes, G., Donis, J., Fridman, J., Hanewinkel, M., Jactel, H., Lindner, M., Marchetti, M., Marušák, R., Sheil, D., Tomé, M., Trasobares, A., Verkerk, P.J., Korhonen, M., Nabuurs, G.-J., 2021. Concerns about reported harvests in European forests. *Nature* 592, E15–E17.
- Pauleus, O., Aide, T.M., 2020. Haiti has more forest than previously reported: land change 2000–2015. *PeerJ* 8, e9919.
- Pengra, B.W., Stehman, S.V., Horton, J.A., Dockter, D.J., Schroeder, T.A., Yang, Z., Cohen, W.B., Healey, S.P., Loveland, T.R., 2020. Quality control and assessment of interpreter consistency of annual land cover reference data in an operational national monitoring program. *Remote Sens. Environ.* 238.
- Poorter, L., Bongers, F., Aide, T.M., Almeyda Zambrano, A.M., Balvanera, P., Becknell, J. M., Boukili, V., Brancalion, P.H.S., Broadbent, E.N., Chazdon, R.L., Craven, D., de Almeida-Cortez, J.S., Cabral, G.A.L., de Jong, B.H.J., Denslow, J.S., Dent, D.H., DeWalt, S.J., Dupuy, J.M., Durán, S.M., Espirito-Santo, M.M., Fandino, M.C., César, R.G., Hall, J.S., Hernandez-Stefanoni, J.L., Jakovac, C.C., Junqueira, A.B., Kennard, D., Letcher, S.G., Licona, J.-C., Lohbeck, M., Marín-Spiotta, E., Martínez-Ramos, M., Massoca, P., Meave, J.A., Mesquita, R., Mora, F., Muñoz, R., Muscarella, R., Nunes, Y.R.F., Ochoa-Gaona, S., de Oliveira, A.A., Orihuela-Belmonte, E., Peña-Claros, M., Pérez-García, E.A., Piotto, D., Powers, J.S., Rodríguez-Velázquez, J., Romero-Pérez, I.E., Ruiz, J., Saldarriaga, J.G., Sanchez-Azofeifa, A., Schwartz, N.B., Steininger, M.K., Swenson, N.G., Toledo, M., Uriarte, M., van Breugel, M., van der Wal, H., Veloso, M.D.M., Vester, H.F.M., Vicentini, A., Vieira, I. C.G., Bentes, T.V., Williamson, G.B., Rozendaal, D.M.A., 2016. Biomass resilience of Neotropical secondary forests. *Nature* 530, 211–214.
- Powell, R.L., Matzke, N., de Souza, C., Clark, M., Numata, I., Hess, L.L., Roberts, D.A., 2004. Sources of error in accuracy assessment of thematic land-cover maps in the Brazilian Amazon. *Remote Sens. Environ.* 90, 221–234.
- Rodrigues-Eklund, G., Hansen, M.C., Tyukavina, A., Stehman, S.V., Hubacek, K., Baiocchi, G., 2021. Sample-based estimation of tree cover change in Haiti using aerial photography: Substantial increase in tree cover between 2002 and 2010. *Forests* 12.
- Sabatini, F.M., Bluhm, H., Kun, Z., Aksenov, D., Atauri, J.A., Buchwald, E., Burrascano, S., Cateau, E., Diku, A., Duarte, I.M., Fernández López, Á.B., Garbarino, M., Grigoriadis, N., Horváth, F., Keren, S., Kitenberga, M., Kiš, A., Kraut, A., Ibsch, P.L., Larrieu, L., Lombardi, F., Matovic, B., Melu, R.N., Meyer, P., Midteng, R., Mikac, S., Mikoláš, M., Mozgeris, G., Panayotov, M., Pisek, R., Nunes, L., Ruete, A., Schickhofer, M., Simovski, B., Stillhard, J., Stojanovic, D., Szwagrzyk, J., Tikkanen, O.-P., Toromani, E., Volosyanchuk, R., Vrška, T., Waldherr, M., Yermokhin, M., Zlatanov, T., Zagidullina, A., Kuemmerle, T., 2021. European primary forest database v2.0. *Sci. Data* 8, 220.
- Sangermano, F., Bol, L., Galvis, P., Gullison, R.E., Hardner, J., Ross, G.S., 2015a. Forest baseline and deforestation map of the Dominican Republic through the analysis of time series of MODIS data. *Data in Brief* 4, 363–367.
- Sangermano, F., Bol, L., Galvis, P., Gullison, R.E., Hardner, J., Ross, G.S., 2015b. Habitat suitability and protection status of four species of amphibians in the Dominican Republic. *Appl. Geogr.* 63, 55–65.
- Seidl, R., Turner, M.G., 2022. Post-disturbance reorganization of forest ecosystems in a changing world. *Proc. Natl. Acad. Sci.* 119, e202190119.
- Souza, C.M., Roberts, D.A., Cochrane, M.A., 2005. Combining spectral and spatial information to map canopy damage from selective logging and forest fires. *Remote Sens. Environ.* 98, 329–343.
- Tollerud, H.J., Zhu, Z., Smith, K., Wellington, D.F., Hussain, R.A., Viola, D., 2023. Toward consistent change detection across irregular remote sensing time series observations. *Remote Sens. Environ.* 285, 113372.
- Tucker, C.J., 1979. Red and photographic infrared linear combinations for monitoring vegetation. *Remote Sens. Environ.* 8, 127–150.
- Turubanova, S., Potapov, P.V., Tyukavina, A., Hansen, M.C., 2018. Ongoing primary forest loss in Brazil, Democratic Republic of the Congo, and Indonesia. *Environ. Res. Lett.* 13, 074028.
- UN, 2022. United Nations: World Population Prospects 2022. Department of Economic and Social Affairs, Population Division.
- UNEP-WCMC, & IUCN, 2023. Protected Planet: The World Database on Protected Areas (WDPA) and World Database on Other Effective Area-based Conservation Measures (WD-OECM) [Online], Jul 2023, Cambridge, UK: UNEP-WCMC and IUCN. Available at: www.protectedplanet.net.
- Vancutsem, C., Achard, F., Pekel, J.F., Vieilledent, G., Carboni, S., Simonetti, D., Galleo, J., Aragão, L.E.O.C., Nasi, R., 2021. Long-term (1990–2019) monitoring of forest cover changes in the humid tropics. *Sci. Adv.* 7, eabe1603.
- Wang, Y., Ziv, G., Adami, M., Mitchard, E., Batterman, S.A., Buermann, W., Schwantes Marimon, B., Marimon Junior, B.H., Matias Reis, S., Rodrigues, D., Galbraith, D., 2019. Mapping tropical disturbed forests using multi-decadal 30 m optical satellite imagery. *Remote Sens. Environ.* 221, 474–488.
- Wang, Y., Ziv, G., Adami, M., Almeida, C.A.D., Antunes, J.F.G., Coutinho, A.C., Esquerdo, J.C.D.M., Gomes, A.R., Galbraith, D., 2020. Upturn in secondary forest clearing buffers primary forest loss in the Brazilian Amazon. *Nat. Sustainabili.* 3, 290–295.
- Weisse, M., Potapov, P., 2021. Assessing Trends in Tree Cover Loss over 20 years of Data. *Global Forest Watch*. <https://www.globalforestwatch.org/blog/data/tree-cover-loss-satellite-data-trend-analysis/>.
- White, J.C., Wulder, M.A., Hermsilla, T., Coops, N.C., Hobart, G.W., 2017. A nationwide annual characterization of 25years of forest disturbance and recovery for Canada using Landsat time series. *Remote Sens. Environ.* 194, 303–321.
- Wilson, J.S., Brothers, T.S., Marcano, E.J., 2001. Remote sensing of spatial and temporal vegetation dynamics in Hispaniola: A comparison of Haiti and the Dominican Republic. *Geocarto Int.* 16, 7–18.
- Zhang, J., Shang, R., Rittenhouse, C., Witharana, C., Zhu, Z., 2021. Evaluating the impacts of models, data density and irregularity on reconstructing and forecasting dense Landsat time series. *Sci. Remote Sens.* 4, 100023.
- Zhang, Y., Woodcock, C.E., Arévalo, P., Olofsson, P., Tang, X., Stanimirova, R., Bullock, E., Tarrio, K.R., Zhu, Z., Friedl, M.A., 2022. A global analysis of the spatial and temporal variability of usable Landsat observations at the pixel scale. *Front. Remote Sens.* 3.
- Zhu, Z., Woodcock, C.E., 2014. Continuous change detection and classification of land cover using all available Landsat data. *Remote Sens. Environ.* 144, 152–171.
- Zhu, Z., Gallant, A.L., Woodcock, C.E., Pengra, B., Olofsson, P., Loveland, T.R., Jin, S., Dahal, D., Yang, L., Auch, R.F., 2016. Optimizing selection of training and auxiliary data for operational land cover classification for the LCMAP initiative. *ISPRS J. Photogramm. Remote Sens.* 122, 206–221.
- Zhu, Z., Zhang, J.X., Yang, Z.Q., Aljaddani, A.H., Cohen, W.B., Qiu, S., Zhou, C.L., 2020. Continuous monitoring of land disturbance based on Landsat time series. *Remote Sens. Environ.* 238.
- Zhu, Z., Qiu, S., Ye, S., 2022. Remote sensing of land change: A multifaceted perspective. *Remote Sens. Environ.* 282.